buildings

MDPI

Review

Effects of Different Types of Fibers on Fresh and Hardened Properties of Cement and Geopolymer-Based 3D Printed Mixtures: A Review

Amir Ramezani, Shahriar Modaresi, Pooria Dashti, Mohammad Rasul GivKashi, Faramarz Moodi * and Ali Akbar Ramezanianpour

Department of Civil and Environmental Engineering, Amirkabir University of Technology, Tehran 1591634311, Iran
* Correspondence: fmoodi@aut.ac.ir

Abstract: Three-dimensional printed concrete (3DPC) is emerging as a new building material. Due to automation, this method dramatically decreases construction time and material wastage while increasing construction quality. Despite the mentioned benefits, this technology faces various issues. Among these issues, the inability to use steel bars for reinforcement and early age cracking because of the low water-to-binder ratio and high amount of binders can be mentioned. In this regard, due to the superior properties of fiber-reinforced concrete (FRC), such as high first crack strength, tensile strength, improvement ductility, and resistance to shrinkage cracking, one of the effective ways to reinforce the mixture of the 3DPC is to use fibers instead of steel bars. Regarding the mentioned issues, the effects of different fibers, such as steel, carbon fibers and so on, on fresh and mechanical properties and dimensional stabilities of hardened concrete have been reviewed. It is predicted that using fibers, especially hybrid fibers, not only covers the deficiencies of initial cracking of 3DPC, but also can be used instead of steel bars; therefore, this material can play a pivotal role in the construction industry's future.

Keywords: 3D printed fiber reinforced concrete; mechanical properties; fresh properties; steel fiber; polymer fibers

check for updates

Citation: Ramezani, A.; Modaresi, S.; Dashti, P.; GivKashi, M.R.; Moodi, F.; Ramezanianpour, A.A. Effects of Different Types of Fibers on Fresh and Hardened Properties of Cement and Geopolymer-Based 3D Printed Mixtures: A Review. *Buildings* **2023**, *13*, 945. https://doi.org/10.3390/buildings13040945

Academic Editors: Zhenhua Duan, Hongzhi Zhang, Yu Chen, Oğuzhan Çopuroğlu, Jie Xu and Jianguang Fang

Received: 10 February 2023
Revised: 3 March 2023
Accepted: 31 March 2023
Published: 2 April 2023

Copyright: © 2023 by the authors. Licensee MDPI, Basel, Switzerland. This article is an open access article distributed under the terms and conditions of the Creative Commons Attribution (CC BY) license (https://creativecommons.org/licenses/by/4.0/).

1. Introduction

Today more than ever, the construction industry must evolve in the same way as the industrial sector. The advancement of the construction industry has always been supported by the standard method of conventional construction [1]. However, as the construction field has grown, challenges have developed, and this industry needs to modernize and adapt. As a result, there is potential for the conventional construction sector to undergo a change and upgrade with the help of 3D printing technology used in the industrial sector [2,3].

The idea of the digital fabrication of concrete was presented in 2004 by Behrokh Khoshnevis, termed 'Contour Crafting' [4]. Later, in 2011, researchers at Loughborough University, UK developed 3DPC by depositing layers of fresh concrete as per the digital structure model [5,6]. The integration of 3D printing into the building construction process has resulted in an innovative new construction technology: 3D printing for buildings. Compared to the time-consuming and expensive method of pouring molds, 3D printing reduces construction costs and increases productivity [7]. In addition, high-end, curving structures that are impossible to construct with other methods are simple to print. Fast progress has been made in this area by more than 30 research organizations throughout the world in the last decade [8]. Since Pegna's groundbreaking work, there has been a general trend toward expanding applications of 3D printing in architectural design all across the world [9]. Due to the limitation of these technologies, 3DPC is generally unable to install a

reinforcing steel bar [10,11]. In addition, 3DPC is exposed to quick shrinkages, which are drying, self-drying and especially plastic shrinkage in the early hours after printing [12–15].

In recent years, the application of FRC in engineering structures has gained worldwide interest because of its superior material properties compared to conventional reinforced concrete, such as its high first-crack [16,17] and tensile strength [18,19], high fracture toughness [20,21], excellent energy absorption capacity [21], improvement of ductility [22–24] and great impact resistance [25–27]. In addition, using fibers in FRC can enhance resistance to shrinkage cracking. Fibers can limit excessive expansion [28–30], improve resistance to the propagation of plastic shrinkage cracking [31,32], and restrain drying shrinkage [33–36]. As a result, there has been a popular trend in using fibers in 3DPC, and many ongoing studies on 3DPC focus on the use of fibers in order to improve properties and remove the limitation of the 3DPC. This review discusses the use of different types of fibers in 3DPC. This paper's key and novel contribution is the critical and comprehensive analysis of 3DPC, which is suitable for construction industries and those working in the concrete structures field.

2. Overview

In recent years, many researchers have published articles about 3DPC. In this regard, the effect of different fibers on fresh and mechanical properties has been investigated. The cited bibliographic references were selected from various sources such as Scopus, Elsevier and Google Scholar. Significant articles were analyzed without considering repetitions. As the summarized statistics in Figure 1 show, more than 40% of articles are related to 2021; therefore, this statistic shows that researchers are currently interested in this field. The primary purpose of this article is to consider the effects of various types of fibers on the properties of 3DPC; therefore, academia and industry can use this review to enhance their information about the role of different fibers in 3DPC. The statistics illustrate that the researchers work with steel fibers more than other fibers; hence, it is an excellent opportunity for other scholars to use other types of fibers. Additionally, the statistics demonstrate that developed countries such as China and Australia are attending this field; thus, investigating the challenges of 3DPC could be an exciting subject for universities in other countries.

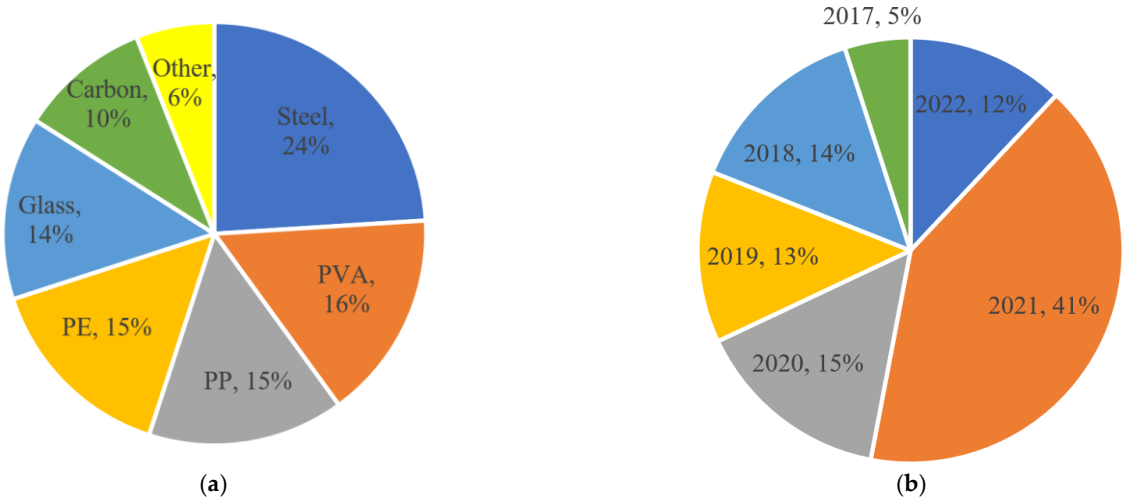
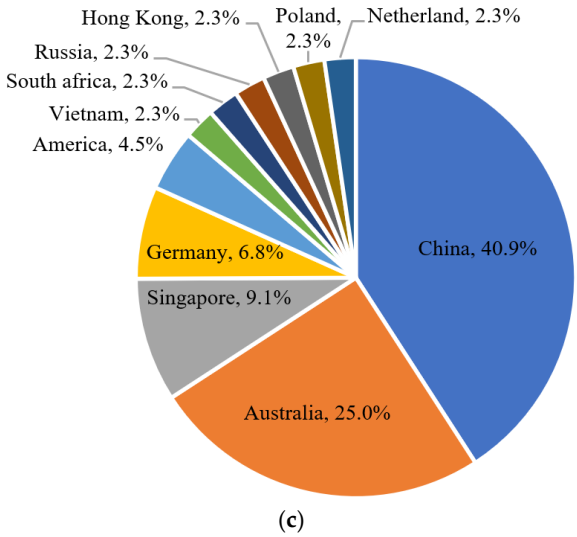


Figure 1. *Cont.*



(**c**)

Figure 1. Summarized statistics about 3DPC: (**a**) Proportion of fibers used in articles; (**b**) Percent of articles published in different years; (**c**) Different countries' participation in the 3DPC essay.

3. Fibers

Fibers that can be used as reinforcements in 3DPC are steel, carbon, glass, polyvinyl alcohol (PVA), polyethylene (PE), and polypropylene (PP). A summary of the typical characteristics of various fibers is shown in Table 1. Different reinforcing fibers might bring various qualities to concrete and play multiple roles in enhancing the functionality of cement-based materials. High-tensile strength fibers such as steel can significantly increase the bending and tensile strength of concrete mixtures, as well as their fatigue and impact resistance. In addition, they can enhance the material's energy absorption capacity, toughness, and strain capacity [37,38]. The downside of steel fibers is that they rust easily and are relatively expensive [39]. Carbon fibers are lightweight, strong, resistant to corrosion, high temperatures, and fatigue, and have a high strength-to-weight ratio. They can also enhance the concrete's electrical conductivity, pressure, and magnetic sensitivity [40–43]. However, they have inadequate impact resistance and weak toughness. Glass fibers offer decent heat insulation and corrosion resistance. Still, they have low alkali resistance and must be coated when used in concrete [44–46]. Polymer fibers are high-strength synthetic monofilament bundle fibers. When these fibers are added to mixtures, they can effectively limit the formation and growth of fractures, as well as increase their impermeability and impact resistance [47]. PVA [48], PE [49], and PP [50] are common types of used synthetic polymer fibers. Other fibers, such as basalt, recycled, and natural, may lessen the brittle failure of composites, but their performance is not as good as that of the mentioned fibers. Therefore, less research has been conducted on using these fibers [51]. Figure 2 shows several types of fibers.

Table 1. Characteristics of fibers. Adapted with permission from [40,52–55].

Fiber Type	Tensile Strength (MPa)	Young's Modulus (GPa)	Elongation (%)	Specific Gravity	Melting Point (°C)
Steel	200–2760	200	0.5–0.35	7.8	1370
PE	690	0.14–0.41	10	0.95	141.4
Glass	1034–3792	72	1.5–3.5	2.5–2.7	860
PVA	1000–1600	22–42	6–7	1.3	220–240
PP	552–690	3.45	25	0.9	170
Carbon	1550–6960	159–965	2.5–3.2	1.8	over 3000
Basalt	872–2800	40–89	3.15	2.8	1500–1700



(**a**) (**b**) (**c**)

Figure 2. Several types of fibers: (**a**) Steel; (**b**) PP; (**c**) Carbon.

4. Fresh Properties

The fresh properties of 3DPC mostly pertain to workability performance. Workability performance includes fluidity, cohesiveness, and water retention. By incorporating fibers into the 3DPC mixtures, it is possible to avoid spalling, restrict deformation and achieve a uniform and continuous printing sample. Furthermore, the key to determining whether the concrete can be continuously and evenly extruded and ensure pouring molding is to manage its thixotropy and setting time due to the needs of the concrete printing process. In addition, it is essential to note that fiber content can block the nozzle when it reaches a sensitive volume [2]. The summarized information about different types of tests in order to determine the fresh concrete properties and their results of them are shown in Table 2.

4.1. Influence of the Steel Fibers

The fresh properties of 3DPC reinforced with steel fibers, length of 13 mm, diameter of 0.2 mm and density of 8.7 kg/m^3, at the contents of 0.25, 0.5, 0.75 and 1 wt.%, were investigated by Singh et al. [56]. In this study, the researchers used natural river sand with a particle size smaller than 1.18 mm and nano clay (nC). The results about the slump flow demonstrated that with the addition of steel fibers, the slump flow decreased. Additionally, when the fiber ratio increased, the slump flow at an early age compared with the control specimen reduced by 4.76, 5.71, 5.71 and 6.61% for specimens that contain 0.25, 0.5, 0.75 and 1 wt.% fibers, respectively. Moreover, adding nano clay increased structural rebuilding during the extrusion of 3DPC because it behaved as an interlocked web, leading to increase in friction and adhesion among particles.

Yang et al. investigated the printing quality of 3D printed ultra-high-performance fiber-reinforced concrete 3DPUHPFRC [57]. The two kinds of round copper-plated steel fibers with a length of 6 and 10 mm were used in the research. Moreover, using the fly ash improved the workability and durability of 3DPC [57]. In this study, the researchers used 24 kg/m^3 nano calcium carbonate in the mix ratio of 3DPUHPFRC so as to improve the properties of the 3D printed paste. The results about the quality of printability illustrated that the 3DPUHPFRC without steel fibers had better quality than that with 1 vol.% 6 mm and 1 vol.% 10 mm steel fibers. This outcome was caused by the difficulties that 3DPUHPFRC had when extruding steel fibers from the nozzle.

4.2. Influence of the PE Fibers

Ye et al. investigated the workability and buildability of 3D printed ultra-high ductile concrete (3DPUHDC) reinforced by PE fibers (1.0, 1.5, and 2.0 vol.%) [58]. 3DPUHDC is a particular type of concrete that is made for its better tensile strain capacity [59–63]. In this research, spread diameter and penetration depth were used in order to evaluate workability. The spread diameter and penetration depth figures for the specimens with 1 vol.% fibers were 169 and 86 mm, respectively. The spread diameter for the samples with 2 vol.% fibers was 144 mm, and the penetration depth was 76 mm. For evaluating printability, the overall

height of the 10-layer was measured. The height of the 10-layer printed samples with 2 and 1 vol.% fibers were 99 and 97 mm, respectively. It was determined that a reduction in the workability occurred because more and more twisted fiber orientation was noticed as the fiber concentration was raised to 1.5 and 2 vol.%.

4.3. Influence of the Glass Fibers

Li et al., investigated the workability and buildability of 3DPC reinforced by glass fibers (up to 0.61 vol.%) [64]. In this research, 3DPC was made from coral sand. In addition, seawater was used for creating 3DPC samples. Freshwater is scarce in remote islands and coastal areas, and shipping from the mainland is prohibitively expensive, posing a significant barrier to concrete manufacturing in these isolated places. In such a case, using saltwater may be a viable option [65–68]. The flow table test was used for workability and buildability; the height of 3DPC was measured. Adding 0.6 vol.% glass fibers reduced the flow diameter and the average height of printed samples by 11 and 11.7 mm, respectively [64]. Chu et al., demonstrated that adding 0.5 vol.% glass fibers into 3D printed high-strength fiber-reinforced concrete (3DPHSFRC) decreased the slump flow and flow diameter by less than 10% [69]. 3DPHSFRC can be engineered to have high tensile strength and flexibility. Moreover, we can replace all steel bars with fibers in 3DPHSFRC [70–73].

4.4. Influence of the PVA Fibers

Sun et al. conducted research that added 0.8, 1, 1.2, 1.4 and 1.6 vol.% PVA fibers in the 3D printed paste [74]. The results about the fluidity illustrated that the addition of PVA fibers decreased the fluidity of the mixture so that the fluidity of the mixture with 0.8 vol.% of PVA fibers was 21% more than that of mixtures with 1.6 vol.% of PVA fibers. In this regard, other scholars concluded that a higher amount of fibers reduced the fluidity because of interlocking and entangling among fibers in mixtures [75,76].

Zhang and Aslani added 1 and 1.5 vol.% PVA fibers and 0.5 and 1 wt.% activated carbon powder in order to determine the optimum mix design [77]. The results of the slump flow of mixtures illustrated that adding more PVA fibers reduced the slump flow. The main reason for this result is that the addition of fibers restricted the movement of aggregates; hence, the slump flow was reduced. The slump flow of mixtures with no PVA fibers was 57% and 44% higher than mixtures with 1 and 1.5 vol.% PVA fibers, respectively.

Sun et al. investigated the 3D printed lightweight engineered cementitious composites by incorporating 1.75% PVA fibers by mass ratio to cement [78]. The slump flow results illustrated that the mixtures' slump flow with 1.75% of PVA was reduced compared to those without fibers. The slump flow of the mixtures without fibers was 80% higher than that of mixtures with 1.75 wt.% fibers. The PVA fibers also decreased the setting time in comparison with mixtures without fibers. Another scholar asserted that this matter is due to fibers overlapping, making a network with each other and causing a reduction in the setting time [79].

The rheological properties of fresh Engineered Cementitious Composite (ECC) are essential in its application in 3DPC. The rheological behaviors determine the pumping ability, extrudability and buildability of 3DP-ECC samples [80,81]. In this regard, Yu et al. evaluated the rheological properties of 3DP-ECC with 26 kg/m^3 PVA fibers, 1026 kg/m^3 fly ash, 345 kg/m^3 silica sand and 30 kg/m^3 ordinary cement [82]. The results showed that spread flow decreased with time. In this case, the results of the shape retention test demonstrate that with passing time, the ability of the mixture in buildability and shape retention test increased.

4.5. Influence of the PP Fibers

The effect of adding PP fibers on the fresh properties of 3DPC was investigated by Tran et al. [83]. In this research, the content of PP fibers varied from 1.35 to 5.4 kg/m^3. This research used the Bingham model to evaluate the plastic viscosity and the dynamic

yield stress [84]. The specimens with 0.22 water-to-binder ratio and 5.4 kg/m^3 PP fibers had 282.3 3 Pa viscosity and 1207.6 Pa dynamic yield stress. It was stated that adding PP fibers increased the plastic viscosity and the dynamic yield stress by nearly 400% and 320%, respectively, because the friction of the particles in the fresh concrete immediately influenced the dynamic yield stress and plastic viscosity.

Furthermore, PP fibers served as the needle aggregate in fresh concrete. Thus, adding more PP fibers increased the needle aggregate, resulting in high friction among aggregates. Figure 3 shows the 3DPC samples in this research.

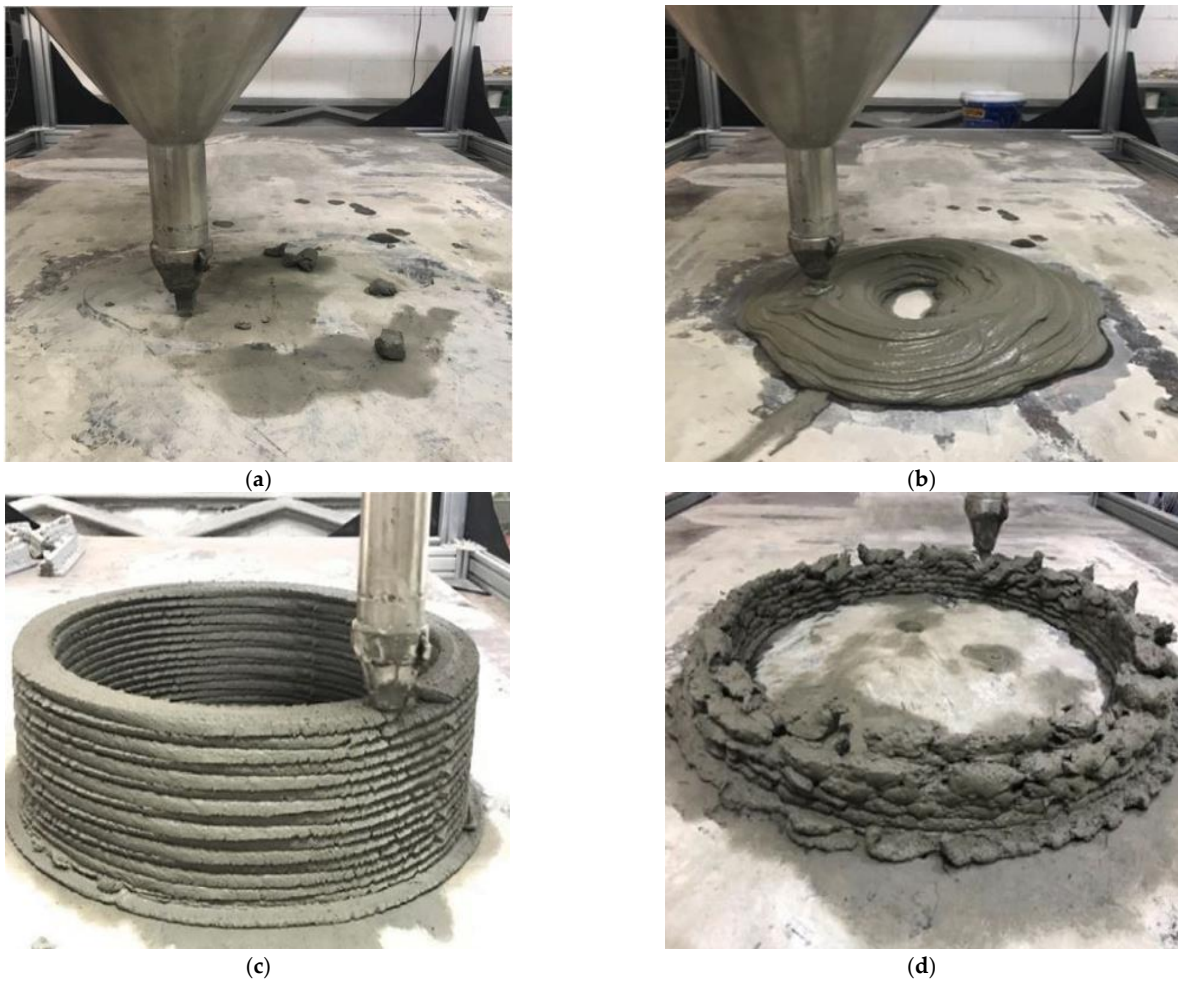


Figure 3. 3DPC samples. (**a**) The 3DPC mixture with low flowability; (**b**) The 3DPC mixture with excessive flowability; (**c**) The 3DPC mixture with proper printability and flowability; (**d**) The 3DPC mixture with low printability and flowability. Adapted with permission of Ref. [83].

4.6. Influence of the Other Fibers

Chu et al. added 0.5 vol.% carbon fibers into 3DPHSFRC and discovered that slump and flow diameter decreased by less than 5% [69]. Li et al. investigated the effect of basalt fibers (0.21, 0.22, 0.42, 0.43, 0.64, 0.65, 0.85 and 0.86 vol.%) on 3DPC. The addition of 0.85 vol.% basalt fibers decreased the flow diameter from 178 to 162 mm. Conversely, the addition of 0.85 vol.% basalt fibers increased buildability from 52.3 to 52.5 mm [64].

4.7. Discussion about Fresh Properties of 3DPC

Table 2 compares the impact of various fiber types on the 3DPC's fresh properties. In this table, the percentage, specifications, and types of fibers are shown. In addition, tests and a summary of the results are provided in Table 2.

Table 2. Comparison of 3DPC mixtures' fresh properties.

Fiber-Reinforced 3DPC							
Type	**Fibers Length**	**Diameter**	**3DPC Mixtures Type**	**Amount of Fiber (%)**	**Tests**	**Results Summary**	**Ref.**
Steel	13 mm	200 μm	3DPC	0.25, 0.5, 0.75 and 1 vol.%	Slump flow	The slump flow decreased by increasing the fiber content.	[56]
Steel	6 and 10 mm	120 μm	3DPUHPFRC	0.25, 0.5, 0.75 and 1 vol.%	Buildability	Mixtures without fibers had more uniform printing than mixtures with fibers.	[57]
Steel	13 mm	200 μm	3DPHSFRC	0.5 vol.%	Slump flow	The flow diameter of mixtures with steel fibers was less than that of mixtures without fibers.	[69]
PP	6 mm	50 μm	3DPC	0.25, 0.5, 0.75, 1, 1.25, 1.5 and 2 vol.%	Viscoelasticity by shear stress	The viscous module increased when the content of fibers increased.	[75]
PP	6 mm	-	3DPC	1.18 kg/m^3	Layer settlement and cylinder stability	There was no visible deformation in the PP fiber mixtures in the layer settlement test. In the cylinder stability test, the average deformation for mixtures containing PP fibers was 31.3 mm.	[80]
PP	6 mm	30 μm	3DPC	1.25, 2.7, 54 kg/m^3	Plastic viscosity and yield stress	The dynamic yield stress increased at equal water-to-binder ratio and superplasticizer dosage with increasing the pp fibers.	[83]
PVA	9 mm	31 μm	3DPC	0.8, 1, 1.2, 1.4 and 1.6 vol.%	Flowability	Flowability was reduced by adding PVA fibers.	[74]
PVA	6 mm	31 μm	3DPC	0.25, 0.5, 0.75, 1, 1.25, 1.5 and 2 vol.%	Viscoelasticity by shear stress	The viscous module increased when the content of fibers increased.	[75]
PVA	12 mm	39 μm	3DPC	1 and 1.5 vol.%	Slump flow	The slump flow decreased by adding fibers.	[77]
PVA	18 mm	39 μm	3DPLWECC	1.75 wt.%	Slump flow and setting time	Both slump flow and setting time were reduced by adding fibers.	[78]
PVA	8 mm	39 μm	3DP-ECC	2 vol.%	Flowability and shape retention	Flowability and shape retention decreased by increasing the time after water addition.	[82]
Glass	12 mm	14–19 μm	3DPC	0.20, 0.21, 0.40, 0.41, 0.60 and 0.61 vol.%	Flow diameter	Increasing the fiber content reduced flow diameter, yet the flow diameter of mixtures with 0.20 vol.% was 9% more than of those without fibers.	[64]
Glass	12 mm	7 μm	3DPHSFRC	0.5 vol.%	Buildability and slump flow	The flow diameter of mixtures with glass fibers was less than of those without fibers.	[69]
Basalt	12 mm	13 μm	3DPC	0.21, 0.22, 0.42, 0.43, 0.64, 0.65, 0.85 and 0.86 vol.%	Flow diameter	Increasing the fiber content reduced the flow diameter of mixtures.	[64]
Carbon	6 mm	7 μm	3DPHSFRC	0.5 vol.%	Buildability and slump flow	In the buildability test, more extrusion pressure was needed for the mixtures with carbon fibers. Slump flow: the flow diameter of mixtures with carbon fibers was less than of those without fibers.	[69]
PE	12 mm	25 μm	3DPUHDC	10, 15 and 20 kg/m^3	Spread diameter and penetration depth	Both spread diameter and penetration depth decreased with increasing the fiber content.	[58]

In most studies, the slump flow test was used for measuring the fresh properties of 3DPC because it is easy to operate and it contains valuable results. As a result, Figure 4 displays the effect of types and percentages of fibers on the slump flow test. As it is seen, the results show that the amount of slump flow for most 3DPC reinforced with fibers was in the range of 150–200 mm, which is consistent with the researchers' findings.

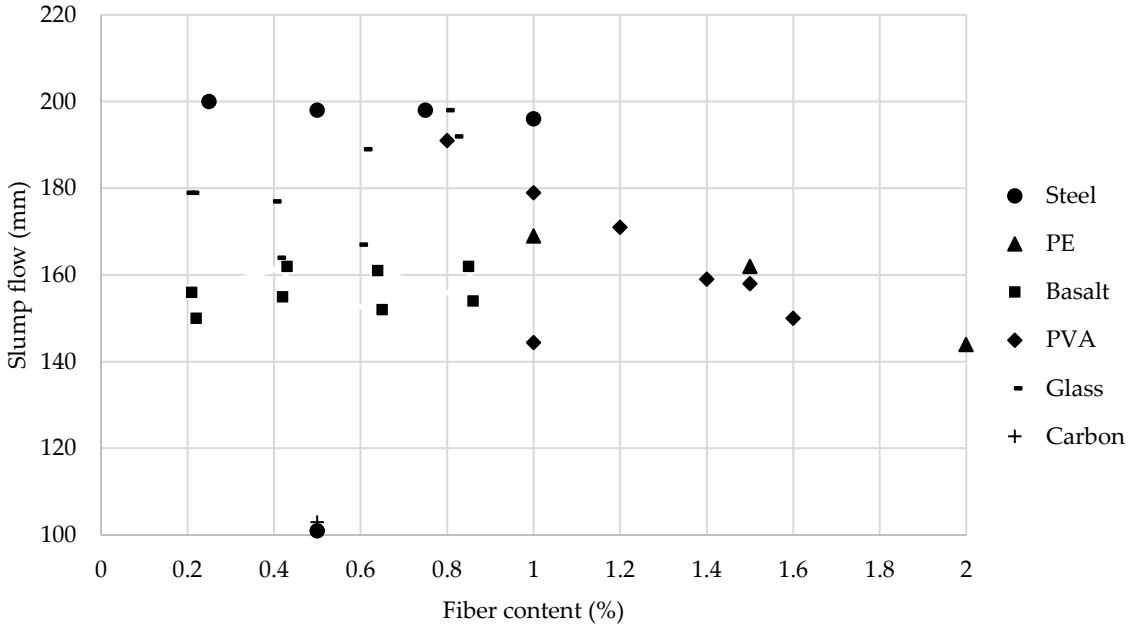


Figure 4. Effect of types and percentage of fibers on the slump flow.

Additionally, the slump flow values and fiber percentage results show that the excessive amount of fibers reduced the slump flow, which can reduce the efficiency of 3DPC, but this is not always the case. The 3DPC's fiber type selection is crucial and may have a negative impact. Basalt and glass fibers seem to improve the slump flow, whereas steel, PE, and PVA decrease it. Based on the fiber type, the rate of changes in the slump flow will also vary. The findings indicate that PVA fibers had a larger slump flow reduction rate than PE and steel fibers. In addition, compared to basalt fibers, the rate of slump flow increased more rapidly for glass fibers.

For steel and basalt fibers, changes in the rate of slump flow were less than 5%, which shows the fiber percentage cannot substantially alter the slump flow. Regarding PE, glass, and PVA fibers, the rate of change in the slump flow was higher and in the range of 25–35%. Finally, PVA fibers seem to have the highest impact on slump flow, while steel fibers have the least impact. Moreover, in most cases, adding fibers generally improved the buildability of mixtures, which is one of the main characteristics of 3DPC.

5. Mechanical Properties

Mechanical properties significantly affect the 3DPC that are loaded in different directions. Compressive, flexural, and tensile strengths are the primary mechanical characteristics of 3DPC. Adding fibers to the 3DPC mixture can have different effects on mechanical properties. However, in most cases, the addition of fibers enhances the mechanical properties. Moreover, the interface bonding strength between different layers of 3DPC is essential. This section provides information about the mechanical properties of 3DPC. In this review, the loading directions to assess the mechanical properties are shown in Figure 5.

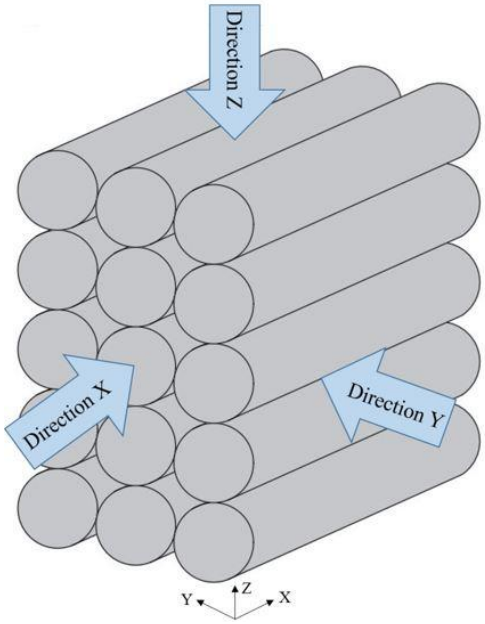


Figure 5. The directions of loading.

5.1. Influence of the Steel Fibers

Arunothayan et al. performed research that assessed the proportion of different contents of steel fibers in 3DPUHPFRC [39]. The results illustrated that the inclusion of steel fibers increased the compressive strength. The results demonstrated that the compressive strength with 1 vol.% steel fibers in the x-direction was 4%, 10%, and 15% higher than that of mold cast specimen, y-direction and z-direction, respectively. Regarding deflection-hardening properties, specimens spanning in y-direction and z-direction had the highest post-peak residual content. Flexural strength in the z-direction was higher than the mold cast specimen in both 1 and 2 vol.% steel fiber content. This result was caused because mold cast specimens contained more random orientation distribution fibers that weakened the flexural properties of concrete compared with 3DPC loaded in the z-direction. It is important to note that mold cast specimen was not printed, and it was the conventional concrete.

Mechanical properties of 3DPC reinforced by steel fibers with different lengths (3 to 6 mm) and varying contents (0.2, 0.5, 0.75, and 1 vol.%) have been investigated by Pham et al. [85]. The result about density illustrated that the density of 3DPC specimens was 2.7% higher than that of mold cast specimens because the extrusion pressure compacts 3DPC specimens rather than the manual compaction of mold cast specimens. In addition, the printed sample in the z-direction displayed 15% higher flexural strength than the mold cast specimen, which was related to the continuous concrete filaments aligning with the length of the beam and well-compacted concrete because of the pressure of extrusion in this direction. Moreover, the steel fibers with a length of 6 mm at contents of 0.25 and 0.5 vol.% had no significant impact on flexural strength because of insufficient fibers in the crossing cracks. In contrast, the steel fibers with 6 mm length at 0.75 and 1 vol.% significantly increased flexural strength. Micro-CT was utilized in order to recognize pores in 3DPC. The results illustrated that the proportion of pores decreased significantly when the steel fiber content increased. In addition, since the extrusion pressure eliminates voids, 3DPC specimens were less porous than mold cast specimens.

According to various studies, increasing the fiber content led to an increase in the compressive strength; however, after reaching a specific optimum content, the fibers negatively affected the compressive strength of 3DPC because of entrapped air by accumulation in the mixture [86,87]. In this regard, Sigh et al. showed that the highest compressive strength for 3DPC belonged to specimens containing 0.75 vol.% steel fibers [56]. The compressive

strength of specimens with 0.75 vol.% steel fibers was 20% higher than that of specimens with 0.25 vol.% steel fibers, and it was also 25% higher than that of specimens with 1% steel fibers. Consequently, the results illustrated that increasing the fiber content higher than the optimum dosage had a negative effect on 3DPC. X-CT observation of 90-degree-oriented samples revealed that lower layers of 3DPC had lower porosity than the top layer due to the compaction of top layers.

The research of Yang et al. about the effect of round copper-plated steel fibers with a length of 6 mm at contents of 0, 0.25, 0.5, 0.75, and 1 vol.% illustrated that the compressive strength of specimens without and with 0.25 vol.% fibers was higher than that of the specimen containing 0.5 vol.% steel fibers [57]. In the same way, the compressive strength of specimens with 0.75 and 1 vol.% steel fibers was higher than that of specimens with 0.5 vol.% steel fibers. In this regard, the authors of the paper mentioned the two effects of steel fibers on 3DPC: (i) increasing the fiber content led to difficulty in pouring printing material, hence resulting in internal defects which caused a reduction in the compressive strength, and (ii) because of increasing fiber content, the effect of restraint of steel fibers increased; consequently, it improved the compressive strength of 3DPC. Therefore, the internal defect was more noticeable in specimens with 0.5 vol.% of fibers; thus, this matter reduced the compressive strength of specimens with 0.5 vol.%.

Some scholars have reported that the compressive strength of mold cast specimens was higher than those of 3D printed samples [88,89]. In this case, Yang et al. discovered that the compressive strength of 3DPUHPFRC with 1 vol.% steel fibers in the z-direction was 91.73% higher than that of the mold cast, and also the compressive of y-direction was 76.14% higher than that of the mold cast [57]. The researchers concluded the flexural strength of 3DPC differed slightly in the x-direction with mixtures without fibers because of the alignment of fibers that did not have any role in flexural strength in the x-direction. The flexural strength of 3DPUHPFRC decreased with increasing steel fiber content with a 10 mm length. The main reason for this is that the steel fibers disrupted the process of extrusion; hence, the quality of printing material decreased, and this matter negatively affected the flexural properties. The splitting tensile strength of 3DPUHPFRC with 1 vol.% steel fibers in the x-direction and y-direction were similar to those without fibers. On the other hand, the splitting tensile at 1 vol.% in the z-direction was 46.6% higher than that of mold cast specimens.

Arunothayan et al. compared the mechanical properties of 3DPUHPFRC with and without fibers [90]. The compressive strength of mold cast specimens was higher than that of 3D printed specimens in any direction because mold cast specimens were vibrated, yet 3D printed specimens were not vibrated and displayed more porosity than mold cast specimens. In addition, the compressive strength of 3D printed specimens with 2 vol.% fibers in the y-direction was 16% higher than that of specimens without fibers. The bulk density result illustrated that the addition of steel fibers increased the bulk density of specimens so that the bulk density of a 3D printed specimen with 2 vol.% fibers was 5% higher than that of a specimen without fibers. The interlayer bond strength of the 3D printed specimen with 2 vol.% steel fibers was 88% higher than that of the specimen without fibers, which illustrated that the fiber orientation was parallel to the surface layer. In addition, the inclusion of fibers improved the interlayer strength.

The eco-friendly 3D printable mixtures with 60 wt.% cement replacement by (i) 60 wt.% fly ash, (ii) 60 wt.% ground granulated blast furnace slag (GGBFS), and (iii) 30 wt.% fly ash and 30 wt.% GGBFS with 157 kg/m^3 steel fibers in all mixtures were evaluated by Arunothayan et al. [91]. The results about compressive strength indicated that 3DPC in the x-direction had higher compressive strength than that in the y-direction and z-direction. For instance, the compressive strength in the x-direction containing 60 wt.% GGBFS was 10% and 11% higher than that in the y-direction and z-direction, respectively. Moreover, the compressive strength of 3D printed specimens made with 30 wt.% fly ash and 30 wt.% GGBFS in the x-direction was 8 and 11% higher than that in the y-direction and z-direction, respectively. The flexural strength of mold cast specimens was less than that in 3D printed

specimens in z-direction and y-direction due to the random orientation of steel fibers in the mold cast specimens contributing to bridging the flexural crack. In this regard, the flexural strengths of the specimens containing 60 wt.% fly ash and 157 kg/m^3 steel fibers in the y-direction and z-direction were higher than mold cast specimens.

Ma et al. used a system to entrain a continuous micro steel cable with a diameter of 1.2 mm into a printing nozzle [92]. The micro steel cable was extruded simultaneously with the 3D printed geopolymer in order to produce a reinforced composite. The results about the flexural characteristics support that the reinforced specimens were better than the non-fiber specimens. This study illustrated that the flexural strength of specimens with micro steel cable was 5.1 times higher than that of non-reinforced 3D printed specimens.

Bos et al. compared the flexural strength of the 3DPC with steel fibers, length of 6 mm and diameter of 0.15 mm [93]. The results showed that 2.1 vol.% of steel fibers increased flexural strength significantly, so the average flexural strength of 3DPC with steel fibers was five times greater than that of specimens without fibers. In addition, the researchers concluded that adding fibers eliminated the detrimental effect of the lack of compaction in 3DPC.

The addition of steel fibers increased the elastic modulus of the concrete [94]. Yang et al. used 1 vol.% copper-plated steel fibers with a diameter of 0.12 mm and 6 and 10 mm lengths in 3DPUHPFRC [95]. The results illustrated that the elastic modulus of concrete with 1 vol.% steel fibers in the length of 6 mm was greater than that of the specimens without fibers. In addition, the elastic modulus of specimens with 1 vol.% steel fibers and a length of 10 mm was greater than that of specimens that had 1 vol.% steel fibers with a length of 6 mm.

Zhou et al. added 0.5 vol.% basalt fibers into all specimens with a variation of steel fibers 2.5, 3.5, and 4 vol.% in 3DPUHPFRC [96]. The CT scanning and stereomicroscope methods were applied to illustrate the fiber distribution. The results showed that most steel fibers were parallel to the print direction. This distribution had a significant role in the mechanical strength, so the flexural strength of specimens with the addition of steel fibers in the z-direction and y-direction increased. However, the incorporation of steel fibers did not significantly affect the x-direction due to the direction of steel fibers. In addition, the compressive strength of specimens with 4 vol.% of steel fibers in the z-direction was 20% higher than that of the y-direction and 50% higher than that of the x-direction.

Lim et al. researched the effects of hybrid fibers on the 3D printed geopolymer [97]. In this research, 0.5 wt.% PVA fibers were used in order to compare the effects of steel cable stainless with diameters of 1, 1.5, and 2 mm in reinforced 3D printed geopolymer and control 3D printed geopolymer (without steel fibers). The flexural strength results of the four-point experiment illustrated that the specimens with 2 mm diameter stainless steel cable had higher flexural strength. The results displayed that the difference between the specimens containing 1.5 mm-diameter stainless steel cable was not notable compared to specimens containing 2 mm-diameter steel cable. As a result, the author mentioned that using the 1.5 mm-diameter steel cable was more optimal.

5.2. Influence of the PE Fibers

Ding et al. investigated the flexural strength of 3DPC reinforced by PE fibers (0.25, 0.5, 1 and 1.4 wt.%) [98]. Furthermore, this research used recycled sand from waste concrete [99]. Four-point test was used to evaluate flexural strength. It was determined that when the fiber content increased from 0.25 to 1.4 wt.%, the flexural strength of the mold cast specimen increased by 381%, and for the specimens loaded in the x-direction, y-direction and z-direction, the flexural strength increased by 420, 412 and 437%, respectively. The influence of fiber content on flexural strength is shown in Figure 6.

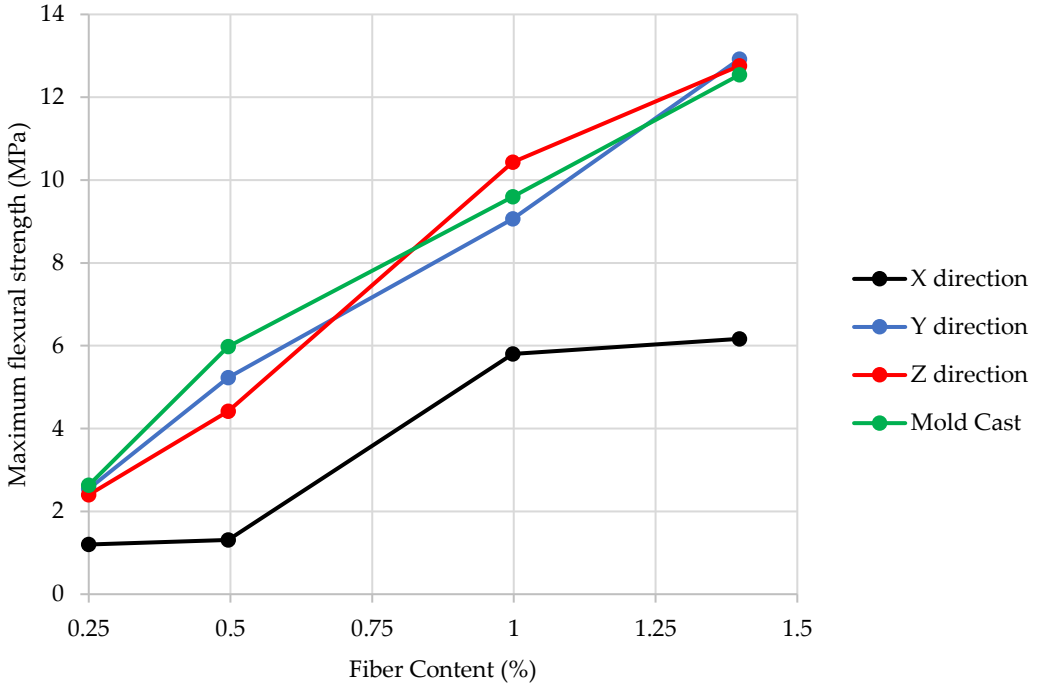


Figure 6. Effect of fiber content on the flexural strength. Adapted with permission of Ref. [98].

Xiao et al. evaluated compressive, flexural, and tensile splitting strength for the 3DPC reinforced by 1% PE fibers (by cement weight) [100]. In addition, in this research, recycled fine aggregates produced from construction and demolition waste were used [101]. For the specimens loaded in the z-direction, the addition of 1% PE fibers (by cement weight) increased compressive strength from 22.1 to 28.6 MPa, tensile splitting strength from 1.91 to 3.23 MPa, and flexural strength from 9.22 to 25.8 MPa. It was stated that adding PE fibers resulted in better mechanical properties owing to the interfacial bond between fibers and the matrix.

Ding et al. investigated the tensile and flexural strength of 3DPC reinforced by PE fibers [102]. This study evaluated the impact of fiber content (0.25, 0.5, 1 and 1.4 wt.%) and fiber length (6 and 12 mm). It was determined that adding 1.4 wt.% PE fibers with 6 mm length into the mold cast specimen increased the flexural strength by 12.38 MPa; for the specimens with 1.4 wt.% PE fibers of 6 mm length and loaded in the x-direction, y-direction and z-direction, the flexural strength rose by 3.89, 8.83 and 7.1 MPa, respectively. The length of PE fibers was determined to have less than a 10% effect on flexural strength. The addition of 1.4 wt.% PE fibers into mold cast specimens increased tensile strength by 3.3 MPa. Flexural strengths in the y-direction and z-direction were the greatest and functioned equally. During the extrusion process, water was lost, and fibers were aligned, increasing the material's strength. In the x-direction, flexural strength was the weakest. The PE fibers did not pass through the printed filaments and did not considerably increase the contact bonding strength. In addition, it was stated that the addition of PE fibers improved mechanical properties because of the interfacial combination between PE fibers and the matrix.

Cai et al. investigated the flexural and compressive strength of 3D printed cementitious composite beams (3DPCCB) reinforced with 1 vol.% PE fibers [103]. The matrix of 3DPC consisted of ordinary Portland cement, silica fume and silica sand. Extrusion devices of steel wire [104], embedded steel mesh [105], and post-tensioning reinforcement [106] are some of the printing methodologies and reinforcing systems for 3DPC structural members that have been documented and designed. According to this study, the average 7-day compressive strength of 3DPCCB cylindrical specimens was 23.2 MPa. The load-bearing capacity for the 3DPCCB, which had joint reinforcement, was 11% lower than 3DPCCB,

which had traditional reinforcements. In this research, a Four-point test was used to evaluate flexural strength.

Ye et al. reported that [58] flexural strength for mold cast, z-direction and y-direction loaded specimens with 2 vol.% PE fibers were 15.1, 14.5 and 14.4 MPa, respectively. The flexural and compressive strengths of 3DPC were examined by Xiao et al. [107]. PE fibers (1% cement weight) and recycled sand were used in this study. Specimens containing 1% wt.% fibers and recycled sand showed a tensile strength of 12 MPa. Moreover, the addition of 1 wt.% fibers increased the compressive strength by approximately 10 MPa.

5.3. Influence of the Glass Fibers

Flexural and compressive strengths of 3DPC reinforced by glass fibers (up to 0.61 vol.%) were evaluated by Li et al. [64]. The addition of 0.2 vol.% glass fibers decreased compressive strength by less than 5% in comparison to the control mixture (without fibers). The flexural strength of printed specimens with 0.2 vol.% of glass fibers was 8.86 MPa, 5% higher than that of printed specimens without fibers. Moreover, with the addition of 0.2 vol.% glass fibers, the compressive strength of specimens decreased by 6%. Shakor et al. investigated the effect of glass fibers on 3DPC [108]. In this research, 1 and 1.5 vol.% glass fibers were used. The addition of 1.5 vol.% fibers increased the compressive strength by 11.52 MPa, but decreased flexural strength by 1.26 MPa. The flexural and compressive strengths of cement paste reinforced by glass fibers were investigated by Hambach et al. [45]. The three-point bending test was used to evaluate flexural strength. The addition of 1 vol.% glass fibers increased flexural strength by 1.8 MPa and decreased compressive strength by 20 MPa. This research reported that printing cement paste composites with effectively aligned glass fibers resulted in a noticeably higher flexural strength for the composites. Lim et al. researched the effect of glass fiber-reinforced polymer (GFRP) on 3DPC [109]. The addition of GFRP increased the max load in the four-point bending test by approximately 500%. There was a minimal increase of about 0.2 and 10 MPa in interlayer bond strength and compressive strength when 0.5 vol.% glass fibers were added to 3DPHSFRC.

Panda et al. studied the effect of adding glass fibers (0.25, 0.5, 0.75 and 1 wt.%) into 3D printed geopolymer mortar [46]. Specimens with 1 wt.% glass fibers (3 mm length) had 5.8, 5.2 and 3.4 MPa flexural strength when loaded in the z-direction, y-direction, and x-direction, respectively. Similarly, specimens loaded in the z-direction, y-direction and x-direction load had 21, 19 and 22 MPa compressive strength, respectively. Tensile strength increased by 0.7 MPa with the addition of 1 wt.% glass fibers (3 mm length) when the loading direction was parallel to the extrusion path. It was determined that because fibers were parallel to the loading direction and behaved as voids depending on the matrix's capacity to tolerate it, this situation affected the compressive strength. In addition, it was stated that interface interaction between fibers and matrix is vital for enhancing the mechanical properties of 3DPC. Jin et al. used the glass fiber mesh, with dimensions of 5×5 mm cut into the size of 70 mm length and 25 mm width (each layer), and glass fiber textile (GFT), to increase the flexural strength of 3D printed cement-based materials [110]. The addition of GFT into specimens increased flexural strength by 608%.

5.4. Influence of the PVA Fibers

The CT images were applied by Sun et al. for the 3DPC with 1.2 vol.% PVA fibers in order to recognize the internal voids and flaws of the layer in printed samples [74]. The results showed that no apparent flaws were detected in the interface layer due to the pressure of the top printing strips. In contrast, poor interfacial contact was observed between some adjacent layers (stripe interface) because of the gaps along the printing direction.

The results illustrated that the compressive strength of specimens with 1.2 vol.% PVA fibers in the z-direction was 5 and 11% more than that in the y-direction and x-direction, respectively. The weakness of compressive strength in the x-direction is due to weakly bounded interfaces parallel to the compressive load [74].

The results of the density of mixtures with PVA fibers were shown by Zhang et al., namely that the density reduced slightly with the addition of the PVA fibers [77]. The results showed that the density of specimens without PVA fibers was 4% higher than that of those with 1.5 vol.% PVA fibers at 28 days. In addition, the flexural strength of printed samples in both z and y-direction was higher than that of cast specimens due to the extrusion of printed concrete from the nozzle, making fiber distribution more uniform than that of cast specimens.

The density of the 3D printed lightweight engineered cementitious composites (3DPLWECC) with the incorporation of PVA fibers at 1.75 wt.% of cement amount was investigated by Sun et al. [78]. The results illustrated that the density of 3DPLWECC after 28 days was 2% higher than that of cast specimens which was due to the squeezing effect of the 3D printed apparatus.

Wang et al. [79] and Ding et al. [102] concluded that the PVA fibers were mechanically oriented parallel to the printing direction with ±20 degrees. This matter positively impacted the flexural toughness of the specimens in the z-direction. In the Sun et al. research, the flexural toughness of 3D printed samples with 1.75 wt.% PVA fibers in the z-direction was 30% higher than that of mold cast specimens [78]. This matter obviously illustrates the positive effect of fiber alignment in the z-direction of 3DPC. In addition, other studies showed that the addition of PVA fibers improved splitting tensile strength and significantly affected cracking resistance as well as pore structure [111,112].

In the research of Yu et al., the compressive strength of mold cast specimens was 31.2 MPa at 28 days, and the compressive strength of 3DPC samples in the y-direction was 30.2 MPa [82]. This result showed that the compressive strength in the y-direction was slightly lower than that of the cast specimens, which explains why the interlayer influence did not have a notable impact on the compressive strength in the y-direction.

Sun et al. researched the compressive and bond properties of 3DPC with 2 vol.% of PVA fibers [113]. It was reported that the compressive strength of the mold cast specimens was 10 and 15% higher than the x-direction and y-direction, respectively. In contrast, the compressive strength of mold cast specimens was slightly higher than that of 3DPC samples in the z-direction. Moreover, the bond strength of 3DPC samples was lower than that of mold cast specimens due to the interlayer and interstrip defects caused by the extrusion during the printing.

Lim et al. studied the effects of hybrid fibers on the 3D printed geopolymer [97]. They used 0.5 wt.% PVA fibers in this research in order to compare the effects of stainless steel cable with a diameter of 1, 1.5 and 2 mm in reinforced 3D printed geopolymer and control 3D printed geopolymer (without steel cable and PVA fibers). The results demonstrated that PVA fibers in printable geopolymer reduced the problems of slippage of the stainless steel cable because of the interaction between short fibers and steel cable.

5.5. Influence of the PP Fibers

Van den Heever et al. investigated the porosity and the compressive capacity of 3DPC reinforced with PP fibers (1 vol.%) [114]. Total porosity for the samples cored in the x-direction and z-direction was 10.3% and 10.8%, respectively. Moreover, the mold cast specimen had 6.5% total porosity. This research stated that PP fibers had a lower density (0.92 kg/m^3) than cement paste (approximately 2150 kg/m^3), so they were seen as voids and were projected to increase the average porosity values by about 1%. The compressive capacity for the samples cored in the x-direction and z-direction was 45.1 and 38.2 MPa, respectively. Moreover, the compressive capacity was 60.5 MPa for the mold cast specimen. Three primary factors, including void topology (shape and direction), localized increases in porosity at interlayer sites and the orientation of interlayer areas in the components of 3DPC, are hypothesized to be the causes of the variances in the respective results.

Nematollahi et al. demonstrated the effects of different volumes of PP fibers on the 3D printed geopolymers [115]. They used fly ash, micron-scale silica sand, an alkaline solution composed of sodium silicate and sodium hydroxide, sodium carboxymethyl cellulose and

PP fibers in four contents of 0.25, 0.5, 0.75 and 1 vol.%. The results about the compressive strength in the z-direction illustrated that the compressive strength of specimens without PP fibers was 22% higher than that of specimens with 1 vol.% of PP fibers, yet the compressive strength of specimens without fibers was 60 and 53% lower than that of specimens that contain 0.25 and 0.5 vol.% PP fibers, respectively. Other scholars interpreted the fact that decreasing the compressive strength with increasing the PP fibers was due to the entrapped air that fibers induced in the mixtures [116,117]. As shown in Figure 7, the flexural strength of the specimen in the z-direction with 0.25 vol.% PP fibers was 9 and 27% higher than those with 0.5 and 0.75 vol.% PP fibers, respectively. This matter illustrated that the higher content of fibers negatively affected flexural strength. On the other hand, the flexural strength of the specimens in the z-direction with 1% PP fibers was 12 and 5% higher than that of specimens with 0.75 and 0.5 vol.% of PP fibers, respectively. The author explained that the fibers had one positive and negative effect on the 3D printed samples. The negative effect is that the fibers induced air in the mixtures, hence decreasing the flexural strength, and the positive effect is that the fibers enhanced the crack bridging capacity. Therefore, in samples with 1% PP fibers, positive effects dominated the negative ones and enhanced flexural strength. Other scholars concluded that adding fibers, regardless of type, reduced the interlayer bond of printed geopolymer [118]. In this regard, Nematollahi et al. compared the interlayer bond of printed geopolymer with 0.25 vol.% PP fibers with specimens that contain 1 vol.% of PP fibers. The results illustrated that the interlayer bond of specimens with 0.25 vol.% PP fibers was 72% higher than that of specimens with 1 vol.% of PP fibers. The author described the reason behind the mixtures containing fibers being stiffer than those without fibers; thus, the printed layer interface for mixtures containing fibers was more porous than those without fibers. This matter led the author to conclude that increasing the fiber content had a negative effect on the interlayer bond strength.

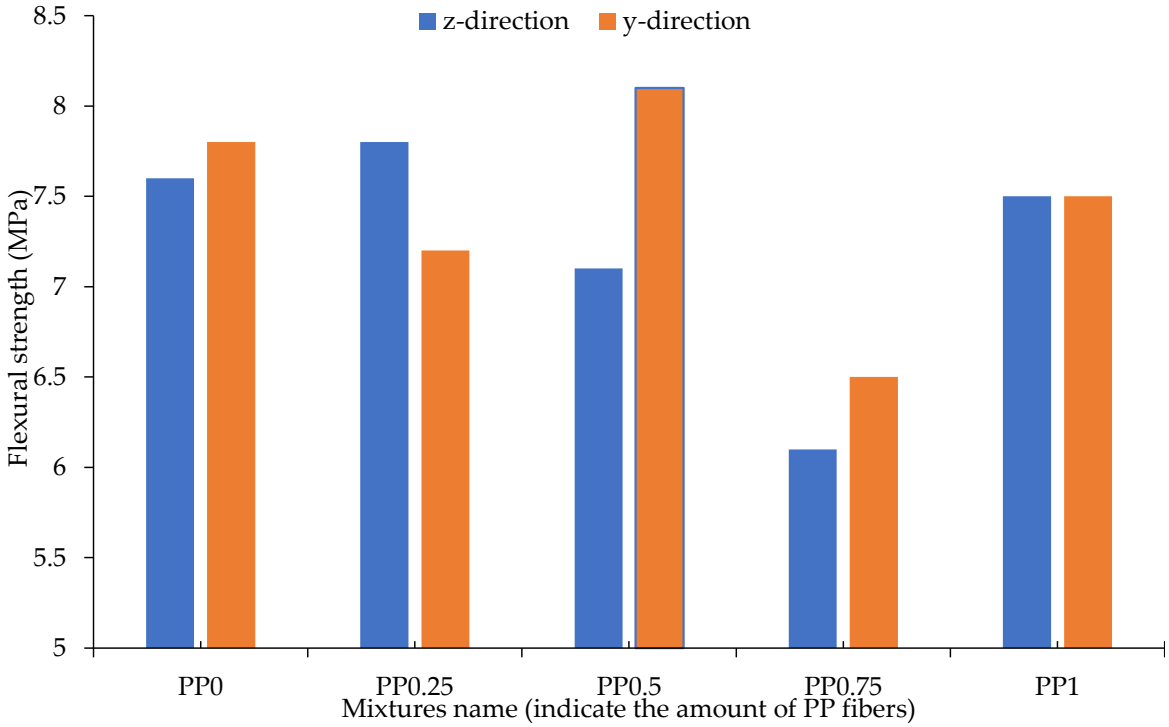


Figure 7. The flexural strength of 3DPC samples in two directions. Adapted with permission of Ref. [115].

Lesovik et al. conducted research to compare the compressive and flexural strengths of specimens containing steel and PP fibers [119]. The results showed that specimens made with hybrid fibers (41.4 kg/m^3 steel fibers and 4.7 kg/m^3 PP fibers) had a 28% higher compressive strength than those made with only 41.4 kg/m^3 steel fibers. In addition, the results showed that the flexural strength of specimens containing hybrid fibers was slightly higher than that of those with only steel fibers.

Nematolahi et al. produced four 3D printed geopolymer specimens: specimens with 0.25 vol.% PP benzobisoxazole (PBO) fibers, 0.25 vol.% PVA fibers, 0.25 vol.% PP fibers, and specimens without fibers in order to compare the flexural strength and interlayer bond of specimens with each other [118]. The results showed that the flexural strength of specimens without fibers was 15, 19 and 26% lower than that of specimens with PP, PVA, and PBO fibers, respectively, due to the effect of fibers which bridged the cracks and contributed to the flexural strength of the 3D printed geopolymer. Moreover, this result was consistent with many published papers on the effect of fibers on flexural and tensile strengths [116,120]. This investigation also illustrated that the flexural strength of specimens with PBO fibers was 14 and 8% higher than that of specimens with PP and PVA fibers, respectively [118]. The main reason for this trend was that PBO fibers' tensile strength and elastic modulus were higher than those of PP and PVA fibers. Interlayer bound of specimens without fibers was 24, 17 and 30% higher than that of specimens with PP, PVA and PBO fibers, respectively, because the incorporation of fibers increased the stiffness of mixtures. As a result, the interlayer of mixtures which contain fibers was more porous than that of specimens without fibers.

Chen et al. researched the effect of PP fibers on the mechanical properties of 3D printed reinforced calcium sulphoaluminate cement composites [75]. The results about the flexural strength showed that with the increase in the PP fiber content, the flexural strength increased, yet increasing the fiber content by more than 1 vol.% decreased the flexural strength. The main reason was that the agglomeration phenomenon occurred with increasing the PP fibers; consequently, it caused some defects in the paste [121,122].

5.6. Influence of the Carbon Fibers

Scheurer et al. investigated the effect of adding carbon fibers into 3DPC on flexural strength [123]. This study used carbon fiber tapes for reinforcing. The spreading method was used to turn carbon fiber rovings into carbon fiber tapes [124]. In this article, each 3DPC specimen was reinforced by three carbon fiber tapes. As a result, the flexural strength of the beams was raised by 125% compared to reference beams reinforced with unspread rovings [123]. The addition of 1 vol.% carbon fibers increased the flexural strength of 3D printed cement paste by 18.5 MPa. Nevertheless, the addition of 1 vol.% carbon fibers reduced compressive strength by 20.5 MPa [45]. Chu et al. determined that interlayer bond and compressive strength increased by less than 10% when 0.5 vol.% carbon fibers reinforced the specimens [69]. Rutzen et al. investigated the effect of different contents of carbon fibers on the mechanical properties of 3DPC. The results illustrated that the flexural strength improved with increasing carbon fibers. Although the printed specimens without fibers showed immediate brittle failure, the addition of fiber improved the loading bearing capacity. In this regard, the flexural strength of printed specimens with 3 vol.% carbon fibers was 81 and 17% higher than that of printed specimens with 2 and 1 vol.% carbon fibers, respectively. As shown in Figure 8, the inclusion of carbon fibers had an essential role in the flexural strength so that the incorporation of 3 vol.% of fibers increased the flexural strength by more than four times in comparison with specimens without fibers. The researchers also observed the effect of carbon fibers on porosity. The content of fibers did not have any effect on the porosity, yet the observation illustrated that the specimens with 2 vol.% and 3 vol.% fiber content had larger pores than specimens with 1 vol.% fibers [125].

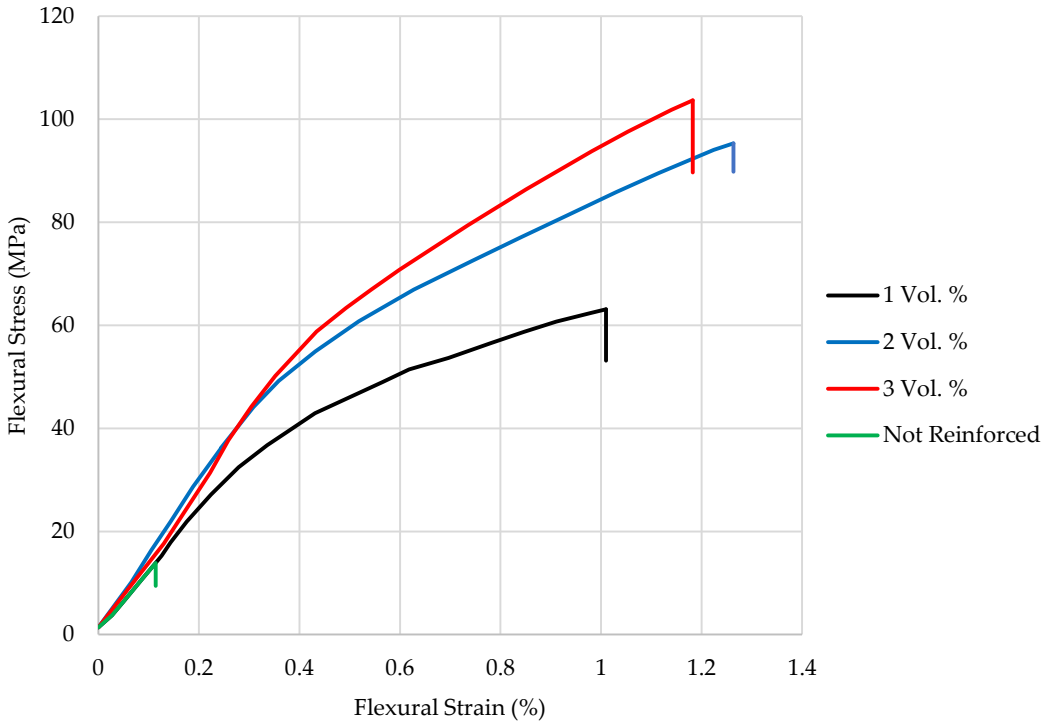


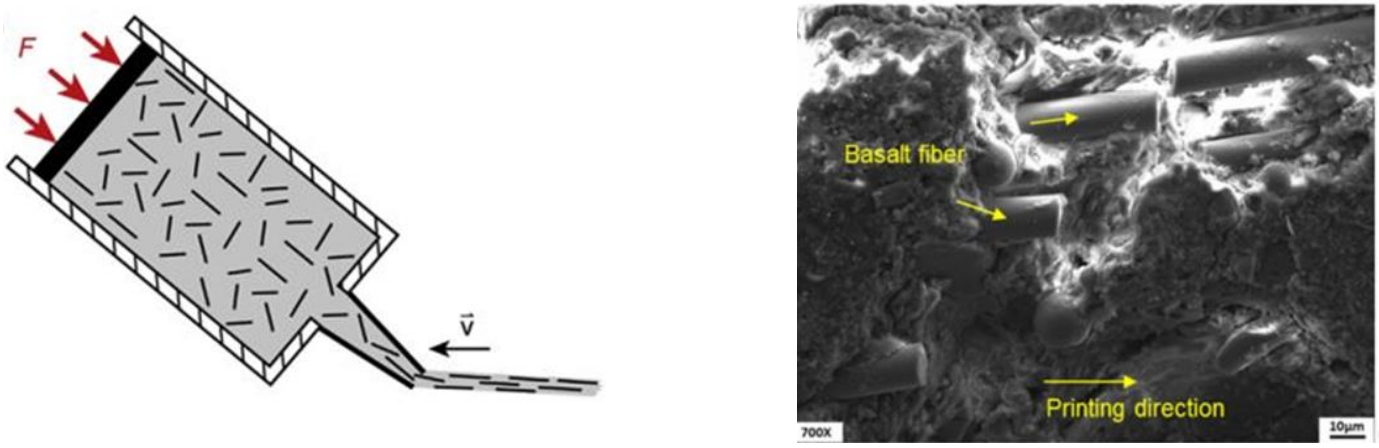
Figure 8. Comparison of flexural strength in different fiber volumes. Adapted with permission of Ref. [125].

5.7. Influence of the Other Fibers

Li et al. evaluated the flexural and compressive strengths of 3DPC reinforced by basalt fibers. The samples with 0.85 vol.% basalt fibers had 7.41 MPa flexural strength and 58.66 MPa compressive strength. The addition of 0.85 vol.% basalt fibers reduced the compressive and flexural strengths by more than 10% compared to the printed specimens without fibers [64]. The addition of 1 vol.% basalt fibers increased the flexural strength of 3D printed cement paste by 3.2 MPa. However, the addition of 1 vol.% basalt fibers negatively affected and reduced compressive strength by 18.1 MPa [45]. Ma et al. investigated the effect of adding basalt fibers (0.1, 0.3, 0.5 and 0.7 wt.%) into the 3DPC with fly ash and silica fume [88]. The flexural strength of the samples with 0.7 wt.% basalt fibers was 4.5 MPa, which was higher than that of specimens with 0.1, 0.3 and 0.5 wt.% basalt fibers by 50%, 36% and 2%, respectively. Moreover, 3D printed samples with 0.5 wt.% basalt fibers had 39.6, 37, and 29.8 MPa compressive strength when loaded in the x-direction, y-direction and z-direction, respectively. In addition, splitting tensile strength for samples with 0.5 wt.% basalt fibers loaded in the x-direction, y-direction and z-direction were 3.62, 3.02, and 5.26 MPa, respectively. This research stated that fiber alignment could enhance mechanical properties. This phenomenon was investigated by SEM test. Figure 9 shows schematic diagrams of nozzle injection and a sizable number of basalt fibers that are mechanically aligned along the print direction.

Korniejenko et al. investigated mechanical properties such as compressive and flexural strengths for the 3D printed geopolymer reinforced with green tow flax fibers [44]. Fly ash, GGBFS and metakaolin are a few industrial wastes or by-products that have been utilized to create geopolymer composites [126,127]. In comparison to typical cement-based composites, geopolymers provide cementless blenders that are more capable and perform better [128]. The Institute of Natural Fibers and Medicinal Plants in Poland, Poznań is where the green tow flax fibers were obtained. A coarse, fragmented fiber called tow is taken out of flax during processing. These fibers, which are semi-products in the manufacture of textile fiber, are typically shorter than 30 cm [129]. The length of the fibers utilized as samples in this investigation ranged from 30 to 50 mm, and samples were created from fly ash.

This research used three production techniques: type 1 was conventional pouring molding with a vibrating table, type 2 was injection molding designed to mimic 3D printing, and type 3 was traditional pouring molding without a vibrating table. The 28-day compressive strength for type 1, 2 and type 3 samples containing flax fibers (1 wt.%) was 40, 48 and 43 MPa, respectively. Type 1 samples had the lowest compressive strength. This effect could be brought on by air bubbles or fiber balling during molding.



(**a**) (**b**)

Figure 9. Effect of printing direction on fibers: (**a**) The direction of fibers in the printing process (schematic image); (**b**) The fibers were aligned in the printing direction (SEM image). Adapted with permission of Ref. [88].

5.8. Discussion about Mechanical Properties of 3DPC

In order to conduct an in-depth discussion, Table 3 is presented, which illustrates the summary of the results on mechanical properties. In this respect, the fiber properties including type, length, diameter, percentage of the fibers used, and the optimal amount of fibers for maximum compressive and flexural strengths are provided. According to the studies, different fibers or combinations of fibers (hybrid) can be used in the 3DPC mixture, which depends on the needed properties. However, Table 3 shows that the researchers used steel fibers more often than the other fibers.

According to Table 3, the highest length-to-diameter (L/D) ratio of steel fibers used in the various studies was around 20% of the other fiber types, while basalt and carbon fibers had the largest L/D ratio. Regarding the percentage of fibers in 3DPC, Table 3 reveals that researchers used 0–2 vol.% of fibers in 3DPC.

Table 3 shows the optimal percentage of fibers for achieving the maximum compressive and flexural strength values based on the studies. Compressive strength in the x and z directions and flexural strength in the z-direction seem to have the highest values.

Based on Table 3, Figure 10 shows the values of the maximum flexural strength in terms of the optimal percentage of fibers and the type of fibers in different studies. At the same time, Figure 11 depicts their compressive strength.

Based on Figure 10, the average percent of optimal fiber content used in the studies was around 1 vol.%, and the average maximum flexural strength was approximately 15 MPa. As a result, future studies may be able to obtain 15 MPa flexural strength by combining 1 vol.% of different types of fibers. Regarding the appropriate proportion of fibers, a smaller amount of basalt and PP fiber (0.5 vol.%) was required to achieve the maximum flexural strength. In contrast, PE fibers required more than 1 vol.% for the highest flexural strength. Moreover, Figure 10 indicates that using steel fibers is more efficient in increasing flexural strength than the other fiber types.

Table 3. Comparison of 3DPC mixtures' mechanical properties.

Fibers			3DPC Mixtures			Fiber-Reinforced 3DPC							
						Max Flexural Strength (MPa)			Max Compressive Strength (MPa)				
Type	Length	Diameter	Type	Max Comp. strength (MPa)	Direction	Amount of Fiber (%)	Fiber Concentration	Strength	Direction	Fiber Concentration	Strength	Direction	Other Tests	Ref.
Steel	6 mm	200 µm	3DPUHPFRC	126.1	x-direction	1 and 2 vol.%	2 vol.%	40	z-direction	2 vol.%	151.2	x-direction	Modulus of rupture	[39]
Steel	13 mm	200 µm	3DPC			0.25, 0.5, 0.75 and 1 wt.%				0.75 wt.% (~0.1 vol.%)	37	y-direction	X-CT	[56]
Steel	6 and 10 mm	120 µm	3DPUHPFRC	120	z-direction	0.25, 0.5, 0.75 and 1 vol.%	1 vol.% with 6 mm	46	z-direction	1 vol.% with 10 mm	152.4	z-direction	Splitting tensile strength	[57]
Steel	13 mm	200 µm	3DPHSFRC	112		0.5 vol.%				0.5 vol.%	128		Interlayer bond strength	[69]
Steel	3 and 6 mm	200 µm	3DPC	90	x-direction	0.25, 0.5, 075 and 1 vol.%	1 vol.%, with 3 mm	15.5	z-direction	0.25 vol.% with 3 mm	112	x-direction	Density and X-ray micro computed tomography analysis	[85]
Steel	13 mm	200 µm	3DPUHPFRC	123.9	x-direction	2 vol.%				2 vol.%	144.2	x-direction	Density and interlayer bond	[90]
Steel	6 mm	200 µm	3DPUHPFRC			157 kg/m^3				157 kg/m^3 (~1.8 vol.%)	166.5	x-direction	Thermal analysis	[91]
Steel	1.2 mm		3D printed geopolymer			0.8 vol.%	0.8 vol.%	30						[92]
Steel	6 mm	150 µm	3DPC			2.1 vol.%	2.1 vol.%	6						[93]
Steel	6 mm		3DPUHPFRC	65	y-direction	2.5, 3.5 and 4 vol.% (hybrid with basalt fibers)	4 vol.% (hybrid)	42	z-direction	4 vol.% (hybrid)	122	z-direction	Micro structure analyses	[96]
Steel	30 mm	300 µm	3DPC	42		41.4 kg/m^3 (hybrid with pp fibers)	41.4 kg/m^3 (~0.53 vol.%) (hybrid)	10		41.4 kg/m^3 (~0.53 vol.%) (hybrid)	92		Plastic strength, water absorption and frost resistance	[119]
PE	12 mm	25 µm	3DPUHDC			1, 1.5 and 2 vol.%	1.5 vol.%	13.3	y-direction	1 vol.%	53.4	x-direction	Tensile strength and micro structure	[58]
PE	6 and 12 mm	20 µm	3DPC			0.25, 0.5, 1 and 1.4 wt.%	1.4 wt.% (~3.5 vol.%)	12.5	y-direction					[98]
PE	12 mm	20 µm	3DPC	31		1 wt.%	1 wt.% (~2.5 vol.%)	15	y-direction	1 wt.% (~2.5 vol.%)	29	z-direction	Macro and micro analysis	[100]
PE	6 and 12 mm	20 µm	3DPC			0.25, 0.5, 1 and 1.4 wt.%	1.4 wt.% with 12 mm (~3.5 vol.%)	13					Micro structure analyses	[102]
PE	12 mm	27 µm	3DPC	25		3.2 kg/m^3	3.2 kg/m^3 (~0.33 vol.%)	13	z-direction	3.2 kg.m^3 (~0.33 vol.%)	35		Pore structure analysis	[107]
PP	6 mm	31 µm	3DPC	52.5		0.25, 0.5, 0.75, 1, 1.25 and 1.5 vol.%	0.75 vol.%	9.5		0.25 vol.%	58		SEM and CT analysis	[75]
PP	6 mm	30 µm	3DPC			1 vol.%				1 vol.%	45	x-direction	Porosity, young's and elasticity modulus	[114]
PP	6 mm	11.2 µm	3D printed geopolymer	24.4	y-direction	0.25, 0.5, 0.75 and 1 vol.%	0.5 vol.%	8.1	y-direction	0.25 vol.%	35.8	z-direction	Apparent porosity and fracture energy	[115]
PP	6 mm	11.2 µm	3D printed geopolymer			0.25 vol.%	0.25 vol.%	9.5					Interlayer bond strength	[118]

Table 3. *Cont.*

Fibers			3DPC Mixtures			Fiber-Reinforced 3DPC							
						Max Flexural Strength (MPa)			Max Compressive Strength (MPa)				
Type	**Length**	**Diameter**	**Type**	**Max Comp. strength (MPa)**	**Direction**	**Amount of Fiber (%)**	**Fiber Concentration**	**Strength**	**Direction**	**Fiber Concentration**	**Strength**	**Direction**	**Other Tests**	**Ref.**
PVA	9 mm	31 µm	3DPC			0.8, 1, 1.2, 1.4 and 1.6 vol.%	1.2 vol.%	14	z-direction	1.2 vol.%	74.16	z-direction		[74]
PVA	6 mm	50 µm	3DPC	52.5		0.25, 0.5, 0.75, 1, 1.25 and 1.5 vol.%	1 vol.%	12.5		0.75 vol.%	67		SEM and CT analysis	[75]
PVA	12 mm	39 µm	3DPC	38.58		1.5 vol.%	1.5 vol.%	10.81	z-direction	1.5 vol.%	45.05	z-direction	Modulus of elasticity	[77]
PVA	18 mm	39 µm	3DPLWECC	40.43		1.75 wt.%	1.75 wt.% (~0.14 vol.%)	9.2	z-direction	1.75 wt.% (~0.14 vol.%)	38	x-direction	Microstructure investigation	[78]
PVA	8 mm	39 µm	3DP-ECC			2 vol.%	2 vol.%	3.38	z-direction	2 vol.%	30.2	y-direction	Interfacial fracture	[82]
PVA	6 mm	26 µm	3D printed geopolymer			0.25 vol.%	0.25 vol.%	9					Interlayer bond strength	[118]
PBO	6 mm	12 µm	3D printed geopolymer			0.25 vol.%	0.25 vol.%	10.3					Interlayer bond strength	[118]
Glass	6 mm	20 µm	Fiber-reinforced cement paste	81.1	z-direction	1 vol.%	1 vol.%	12.4	z-direction	1 vol.%	84.5	z-direction	Density, porosity, flexural and compressive modulus	[45]
Glass	3 mm 6 mm 8 mm		3D printed geopolymer			0.25, 0.5, 0.75 and 1 vol.%	1 vol.% 1 vol.% 1 vol.%	5.8 6.2 7	z-direction y-direction z-direction	0.25 vol.%	27 (just 3 mm)	x-direction		[110]
Glass		14–19 µm	3DPC	89.56		0.2, 0.21, 0.41, 0.6 and 0.61 vol.%	0.4 vol.%	10.02		0.21 vol.%	88.93			[64]
Glass	12 mm	7 µm	3DPC	112		0.5 vol.%				0.5 vol.%	123		Interlayer bond strength	[69]
Basalt	6 mm	13 µm	Fiber-reinforced cement paste	81.1	z-direction	1 vol.%	1 vol.%	13.8	z-direction	1 vol.%	85	z-direction	Density, porosity, flexural and compressive modulus	[45]
Basalt	12 mm	13 µm	3DPC	89.56		0.21, 0.22, 0.42, 0.43, 0.64, 0.65, 0.85 and 0.86 vol.%	0.22 vol.%	9.24		0.43 vol.%	85.32			[64]
Basalt	18 mm	12–15 µm	3DPC			0.1, 0.3, 0.5 and 0.7 wt.%	0.7 wt.%	6	z-direction	0.7 wt.%	40	x-direction		[88]
Carbon	5 mm	8 µm	3D printed geopolymer	50.5		1 wt.%	1 wt.% (~1.25 vol.%)	8.3		1 wt.% (~1.25 vol.%)	50			[44]
Carbon	3 mm	7 µm	Fiber-reinforced cement paste	81.1	z- direction	1 vol.%	1 vol.%	29.1	z-direction	1 vol.%	82.3	z-direction	Density, porosity, flexural and compressive modulus	[45]
Carbon	6 mm	7 µm	3DPC	112		0.5 vol.%				0.5 vol.%	122		Interlayer bond strength	[69]

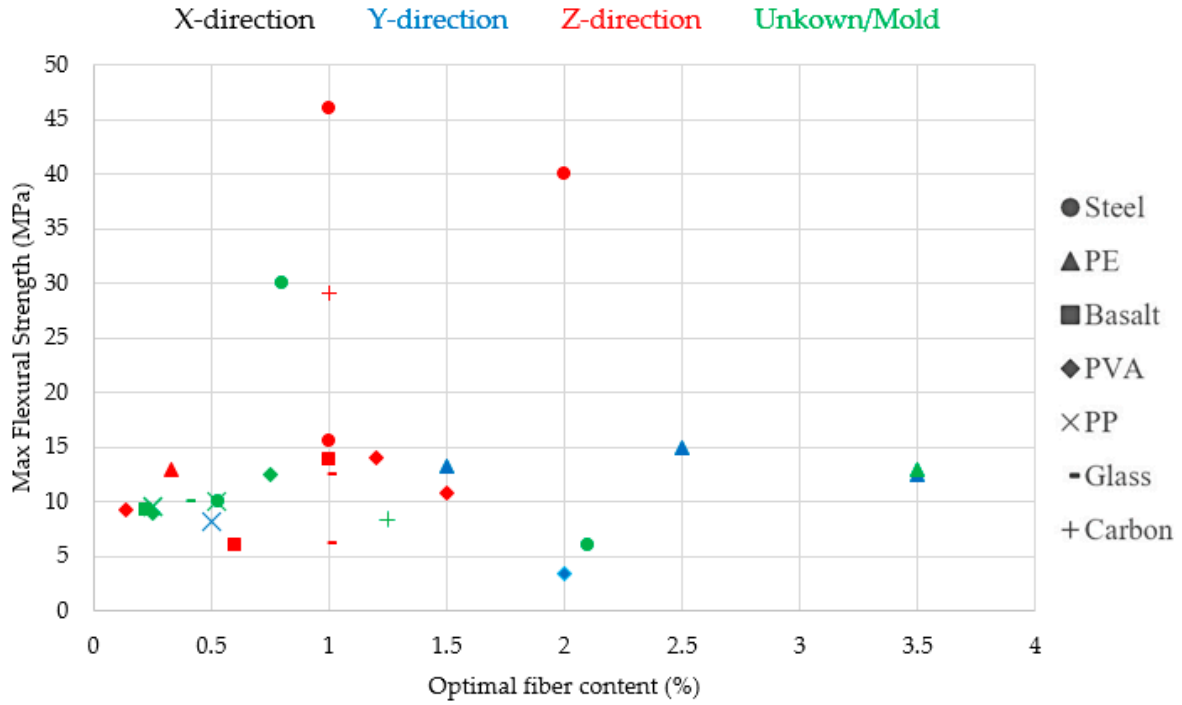


Figure 10. Values of the maximum flexural strength based on the optimal (volume) percentage and type of fibers in different studies.

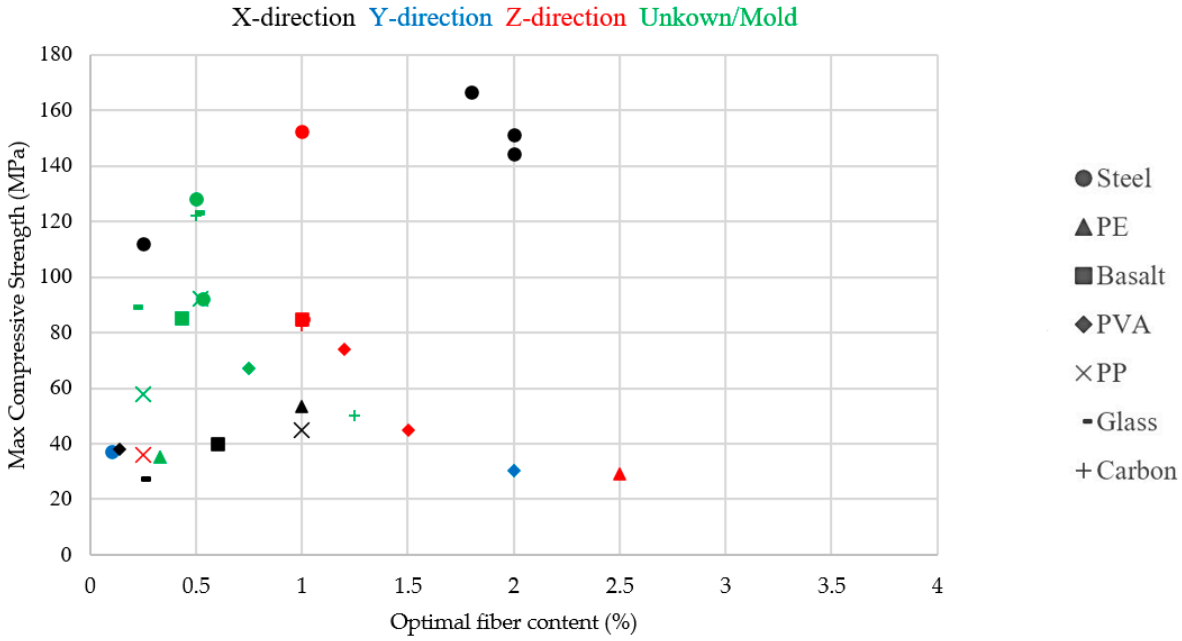


Figure 11. Values of the maximum compressive strength based on the optimal (volume) percentage and type of fibers in different studies.

Similarly to the previous description, based on Figure 11, the average fiber content for the maximum compressive strength was around 1% vol., and the average compressive strength in the experiments was approximately 80 MPa. The range of maximum compressive strength for several studies was quite broad, making it impossible to draw precise conclusions.

It seems that the optimal percentage of glass and PP fibers was smaller than that of other fibers and was around 0.5% vol., while the optimal percentage of PE fibers was more than 2% vol.

In the end, steel fiber had more effect on the compressive strength, and PE, PVA, and PP fibers had the least impact on compressive strength.

6. Dimensional Stability

3DPCs often have high amounts of binder, which is a mix of cement and supplementary cementitious materials. They also typically have low water-to-binder ratios and fine aggregate with a D_{max} of 2 mm. These concrete mixtures produce compacted structures with fine-grained compositions, which aid in maintaining their shape and exhibit a quick setting time. However, the mix proportions and the 3D printing technique provide difficulty since in the early hours after printing, printed concrete structures are vulnerable to rapid shrinkages caused by drying, self-drying, and mainly plastic shrinkage [12].

Influence of the PP Fibers

Tran et al. evaluated shrinkages for 3DPC reinforced with PP fibers [83]. The specimens with 0.26 water-to-binder ratio and 1.35 Kg/m^3 PP fibers had 62.12 maximum strain ($\mu\varepsilon$). Strain at 12 and 24 h for those samples were 62 and 81%, respectively. Samples without PP fibers and the same water-to-binder ratio had 46.35 maximum strain ($\mu\varepsilon$). In addition, strain at 12 and 24 h was 66 and 83%, respectively. The mixture's flow was also reduced because of the PVA fiber addition.

7. Conclusions

The fibers are the main part of the 3DPC. In this regard, the effects of PP, PVA, steel, PE, and carbon fibers on the fresh and mechanical properties of 3DPC have been investigated. The summarized results are elaborated on below.

- Based on the articles, the incorporation of steel fibers increased flexural and compressive strengths. However, the use of more than the recommended dosage resulted in negative impacts. Additionally, all the articles agreed that the increase in the steel fiber content reduced the slump flow and the ability to extrude the 3D printed paste.
- According to the previous investigations about the effects of using fibers on 3DPC, the addition of about 1 vol.% of PVA fibers increased both flexural and compressive strengths in the z-direction. The slump flow of mixtures was also reduced because of the PVA fiber addition. Moreover, PVA fibers had significant effects on crack resistance and pore structures.
- The use of PP fibers had both positive and negative effects on the 3DPC. The positive one is that PP fibers increased the mixture's ability to bridge the cracks, and the negative one is that the fibers introduced the entrapped air to the mixture. Therefore, it is essential to determine the optimum dosage of fibers in order to obtain the highest flexural capacity and an economical mixture. Moreover, PP fibers improved the dimensional stability of 3DPC and reduced the shrinkage of mixtures.
- In recent studies, PE fibers have been determined to impact flexural strength positively, so specimens with 1.4 vol.% PE fibers had greater flexural strength than those without fibers. Furthermore, the increase in the content of PE fibers increased the risk of twisting the fibers; consequently, this matter decreased the slump flow and workability of mixtures.
- The investigations indicated that the addition of glass fibers did not significantly affect the mechanical properties of 3DPC. Moreover, glass fibers reduced slump flow and negatively affected the fresh properties of 3DPC.
- Recent studies illustrated that the addition of carbon fibers increased flexural strength, but it had a negative effect on compressive strength. The investigation displayed that increase in the carbon fiber content did not affect the porosity, but incorporation of more carbon fibers increased the size of pores in the specimens.

- Based on studies about the incorporation of fibers in 3DPC, the alignment of force in the z-direction was perpendicular to the fibers; consequently, the flexural strength was improved by adding the fibers.

Finally, it seems that to achieve the maximum mechanical properties of 3DPC, the use of 1% vol. of different fibers is the optimal choice. In addition, the results showed that the fresh properties of 3DPC, especially the slump flow, containing 1% volume of various fibers were within the acceptable range. Therefore, it can be said that the choice of 1% vol. fibers can be the best option in terms of mechanical and fresh properties.

8. Recommendation for Future Research

Based on this review, several research topics are determined and recommended. It is suggested that researchers in the future should investigate these topics.

- Effect of different types of fibers such as carbon, steel, PP and PE fibers on dimensional stability (autogenous shrinkage, drying shrinkage, etc.) of 3DPC.
- Using hybrid fiber such as a combination of steel and PP fibers or PVA and carbon fibers in order to evaluate fresh, mechanical properties and dimensional stability of 3DPC.
- Evaluating the effect of each type of fiber with different L/D features on the fresh, mechanical properties and dimensional stability of 3DPC.
- Defining a standard for testing the fresh properties parameters such as buildability and extrudability of 3DPC.
- Conducting studies on the effects of recycled fibers, such as metal chips and waste tire fibers, on the fresh, mechanical properties and dimensional stability of 3DPC.
- Using further microstructure tests, such as SEM, to evaluate the interface condition between the fibers and the binder paste.
- Evaluating the effect of adding carbon and PVA fibers on the fresh properties of 3DPC.
- Studying the incorporation of natural pozzolans on the fresh and mechanical properties of 3DPC.
- Assessing the durability of 3DPC exposed to harsh environments such as chloride ion penetration and carbonic acid penetration.

Author Contributions: Conceptualization, A.A.R., A.R. and P.D.; methodology, A.R., S.M. and P.D.; investigation, A.R., S.M., M.R.G. and P.D.; data curation, A.R., S.M. and P.D.; writing original draft preparation, A.R., S.M., M.R.G. and P.D.; writing—review and editing, F.M., A.R., P.D. and A.A.R.; supervision, F.M. and A.A.R.; project administration, F.M. and A.A.R. All authors have read and agreed to the published version of the manuscript.

Funding: This research received no external funding.

Institutional Review Board Statement: Not applicable.

Informed Consent Statement: Not applicable.

Data Availability Statement: Data can be accessed by contacting the following email address: amir_ramezani@aut.ac.ir.

Conflicts of Interest: The authors declare no conflict of interest.

References

1. Kedir, F.; Hall, D.M. Resource efficiency in industrialized housing construction—A systematic review of current performance and future opportunities. *J. Clean. Prod.* **2021**, *286*, 125443. [CrossRef]
2. Souza, M.T.; Ferreira, I.M.; de Moraes, E.G.; Senff, L.; de Oliveira, A.P.N. 3D printed concrete for large-scale buildings: An overview of rheology, printing parameters, chemical admixtures, reinforcements, and economic and environmental prospects. *J. Build. Eng.* **2020**, *32*, 101833. [CrossRef]
3. Xu, J.; Ding, L.; Love, P.E. Digital reproduction of historical building ornamental components: From 3D scanning to 3D printing. *Autom. Constr.* **2017**, *76*, 85–96. [CrossRef]

4. Khoshnevis, B. Automated construction by contour crafting—Related robotics and information technologies. *Autom. Constr.* **2004**, *13*, 5–19. [CrossRef]
5. Nguyen-Van, V.; Panda, B.; Zhang, G.; Nguyen-Xuan, H.; Tran, P. Digital design computing and modelling for 3-D concrete printing. *Autom. Constr.* **2021**, *123*, 103529. [CrossRef]
6. Panda, B.; Lim, J.H.; Mohamed, N.A.N.; Paul, S.C.; Tay, Y.W.D.; Tan, M.J. Automation of robotic concrete printing using feedback control system. In Proceedings of the ISARC, International Symposium on Automation and Robotics in Construction, Taipei, Taiwan, 28 June–1 July 2017.
7. Conner, B.P.; Manogharan, G.P.; Martof, A.N.; Rodomsky, L.M.; Rodomsky, C.M.; Jordan, D.C.; Limperos, J.W. Making sense of 3-D printing: Creating a map of additive manufacturing products and services. *Addit. Manuf.* **2014**, *1*, 64–76. [CrossRef]
8. Lowke, D.; Dini, E.; Perrot, A.; Weger, D.; Gehlen, C.; Dillenburger, B. Particle-bed 3D printing in concrete construction–possibilities and challenges. *Cem. Concr. Res.* **2018**, *112*, 50–65. [CrossRef]
9. Pegna, J. Exploratory investigation of solid freeform construction. *Autom. Constr.* **1997**, *5*, 427–437. [CrossRef]
10. Le, T.T.; Austin, S.A.; Lim, S.; Buswell, R.A.; Gibb, A.G.; Thorpe, T. Mix design and fresh properties for high-performance printing concrete. *Mater. Struct.* **2012**, *45*, 1221–1232. [CrossRef]
11. Paul, S.C.; Tay, Y.W.D.; Panda, B.; Tan, M.J. Fresh and hardened properties of 3D printable cementitious materials for building and construction. *Arch. Civ. Mech. Eng.* **2018**, *18*, 311–319. [CrossRef]
12. Federowicz, K.; Kaszyńska, M.; Zieliński, A.; Hoffmann, M. Effect of curing methods on shrinkage development in 3D-printed concrete. *Materials* **2020**, *13*, 2590. [CrossRef]
13. Tiberti, G.; Mudadu, A.; Barragan, B.; Plizzari, G. Shrinkage Cracking of Concrete Slabs-On-Grade: A Numerical Parametric Study. *Fibers* **2018**, *6*, 64. [CrossRef]
14. Sayahi, F. *Plastic Shrinkage Cracking in Concrete: Mitigation and Modelling*; Luleå University of Technology: Luleå, Sweden, 2019.
15. Moelich, G.; Kruger, P.; Combrinck, R. A plastic shrinkage cracking risk model for 3D printed concrete exposed to different environments. *Cem. Concr. Compos.* **2022**, *130*, 104516. [CrossRef]
16. Branston, J.; Das, S.; Kenno, S.Y.; Taylor, C. Mechanical behaviour of basalt fibre reinforced concrete. *Constr. Build. Mater.* **2016**, *124*, 878–886.
17. Ramesh, B.; Eswari, S. Mechanical behaviour of basalt fibre reinforced concrete: An experimental study. *Mater. Today Proc.* **2021**, *43*, 2317–2322. [CrossRef]
18. Kang, S.-T.; Choi, J.-I.; Koh, K.-T.; Lee, K.S.; Lee, B.Y. Hybrid effects of steel fiber and microfiber on the tensile behavior of ultra-high performance concrete. *Compos. Struct.* **2016**, *145*, 37–42. [CrossRef]
19. Larisa, U.; Solbon, L.; Sergei, B. Fiber-reinforced concrete with mineral fibers and nanosilica. *Procedia Eng.* **2017**, *195*, 147–154. [CrossRef]
20. Khan, M.; Ali, M. Use of glass and nylon fibers in concrete for controlling early age micro cracking in bridge decks. *Constr. Build. Mater.* **2016**, *125*, 800–808. [CrossRef]
21. Solhmirzaei, R.; Kodur, V. Modeling the response of ultra high performance fiber reinforced concrete beams. *Procedia Eng.* **2017**, *210*, 211–219. [CrossRef]
22. Banthia, N.; Nandakumar, N. Crack growth resistance of hybrid fiber reinforced cement composites. *Cem. Concr. Compos.* **2003**, *25*, 3–9. [CrossRef]
23. Banthia, N.; Gupta, R. Influence of polypropylene fiber geometry on plastic shrinkage cracking in concrete. *Cem. Concr. Res.* **2006**, *36*, 1263–1267. [CrossRef]
24. Huang, K.; Deng, M.; Mo, L.; Wang, Y. Early age stability of concrete pavement by using hybrid fiber together with MgO expansion agent in high altitude locality. *Constr. Build. Mater.* **2013**, *48*, 685–690.
25. Yang, L.; Lin, X.; Gravina, R. Evaluation of dynamic increase factor models for steel fibre reinforced concrete. *Constr. Build. Mater.* **2018**, *190*, 632–644.
26. Yang, L.; Lin, X.; Li, H.; Gravina, R. A new constitutive model for steel fibre reinforced concrete subjected to dynamic loads. *Compos. Struct.* **2019**, *221*, 110849.
27. Yang, L.; Qi, C.; Lin, X.; Li, J.; Dong, X. Prediction of dynamic increase factor for steel fibre reinforced concrete using a hybrid artificial intelligence model. *Eng. Struct.* **2019**, *189*, 309–318.
28. Corinaldesi, V.; Nardinocchi, A. Influence of type of fibers on the properties of high performance cement-based composites. *Constr. Build. Mater.* **2016**, *107*, 321–331. [CrossRef]
29. He, H.A.; Dong, W.; Wu, Z.M. Study on long-term expansive deformation of self-stressing concrete with combined restrictions of steel fibers and steel bar. *Key Eng. Mater.* **2011**, *452*, 533–536. [CrossRef]
30. Gong, J.; Zeng, W.; Zhang, W. Influence of shrinkage-reducing agent and polypropylene fiber on shrinkage of ceramsite concrete. *Constr. Build. Mater.* **2018**, *159*, 155–163.
31. Bertelsen, I.; Ottosen, L.; Fischer, G. Influence of fibre characteristics on plastic shrinkage cracking in cement-based materials: A review. *Constr. Build. Mater.* **2020**, *230*, 116769.
32. Soroushian, P.; Mirza, F.; Alhozajiny, A. Plastic shrinkage cracking of polypropylene fiber reinforced concrete. *Mater. J.* **1993**, *92*, 553–560.
33. Voigt, T.; Bui, V.K.; Shah, S.P. Drying shrinkage of concrete reinforced with fibers and welded-wire fabric. *Mater. J.* **2004**, *101*, 233–241.

34. Banthia, N.; Yan, C.; Mindess, S. Restrained shrinkage cracking in fiber reinforced concrete: A novel test technique. *Cem. Concr. Compos.* **1996**, *26*, 9–14. [CrossRef]
35. Güneyisi, E.; Gesoğlu, M.; Mohamadameen, A.; Alzeebaree, R.; Algın, Z.; Mermerdaş, K. Enhancement of shrinkage behavior of lightweight aggregate concretes by shrinkage reducing admixture and fiber reinforcement. *Constr. Build. Mater.* **2014**, *54*, 91–98. [CrossRef]
36. Koh, K.; Ryu, G.; Kang, S.; Park, J.; Kim, S. Shrinkage properties of ultra-high performance concrete (UHPC). *Adv. Sci. Lett.* **2011**, *4*, 948–952.
37. Ríos, J.D.; Leiva, C.; Ariza, M.; Seitl, S.; Cifuentes, H. Analysis of the tensile fracture properties of ultra-high-strength fiber-reinforced concrete with different types of steel fibers by X-ray tomography. *Mater. Des.* **2019**, *165*, 107582.
38. Zheng, W.; Luo, B.; Wang, Y. Compressive and tensile properties of reactive powder concrete with steel fibres at elevated temperatures. *Constr. Build. Mater.* **2013**, *41*, 844–851. [CrossRef]
39. Arunothayan, A.R.; Nematollahi, B.; Ranade, R.; Bong, S.H.; Sanjayan, J.G.; Khayat, K.H. Fiber orientation effects on ultra-high performance concrete formed by 3D printing. *Cem. Concr. Res.* **2021**, *143*, 106384.
40. Schneider, K.; Michel, A.; Liebscher, M.; Terreri, L.; Hempel, S.; Mechtcherine, V. Mineral-impregnated carbon fibre reinforcement for high temperature resistance of thin-walled concrete structures. *Cem. Concr. Compos.* **2019**, *97*, 68–77. [CrossRef]
41. Goldfeld, Y.; Rabinovitch, O.; Fishbain, B.; Quadflieg, T.; Gries, T. Sensory carbon fiber based textile-reinforced concrete for smart structures. *J. Intell. Mater. Syst. Struct.* **2016**, *27*, 469–489. [CrossRef]
42. Chen, M.; Gao, P.; Geng, F.; Zhang, L.; Liu, H. Mechanical and smart properties of carbon fiber and graphite conductive concrete for internal damage monitoring of structure. *Constr. Build. Mater.* **2017**, *142*, 320–327. [CrossRef]
43. Sassani, A.; Ceylan, H.; Kim, S.; Gopalakrishnan, K.; Arabzadeh, A.; Taylor, P. Influence of mix design variables on engineering properties of carbon fiber-modified electrically conductive concrete. *Constr. Build. Mater.* **2017**, *152*, 168–181.
44. Korniejenko, K.; Łach, M.; Chou, S.-Y.; Lin, W.-T.; Cheng, A.; Hebdowska-Krupa, M.; Gądek, S.; Mikuła, J. Mechanical properties of short fiber-reinforced geopolymers made by casted and 3D printing methods: A comparative study. *Materials* **2020**, *13*, 579. [CrossRef]
45. Hambach, M.; Rutzen, M.; Volkmer, D. Properties of 3D-printed fiber-reinforced Portland cement paste. In *3D Concrete Printing Technology*; Elsevier: Oxford, UK, 2019; pp. 73–113.
46. Panda, B.; Paul, S.C.; Tan, M.J. Anisotropic mechanical performance of 3D printed fiber reinforced sustainable construction material. *Mater. Lett.* **2017**, *209*, 146–149. [CrossRef]
47. Panda, B.; Unluer, C.; Tan, M.J. Investigation of the rheology and strength of geopolymer mixtures for extrusion-based 3D printing. *Cem. Concr. Compos.* **2018**, *94*, 307–314. [CrossRef]
48. Yang, E.-H.; Li, V.C. Strain-hardening fiber cement optimization and component tailoring by means of a micromechanical model. *Constr. Build. Mater.* **2010**, *24*, 130–139. [CrossRef]
49. Yu, K.-Q.; Yu, J.-T.; Dai, J.-G.; Lu, Z.-D.; Shah, S.P. Development of ultra-high performance engineered cementitious composites using polyethylene (PE) fibers. *Constr. Build. Mater.* **2018**, *158*, 217–227. [CrossRef]
50. Panda, B.; Paul, S.C.; Hui, L.J.; Tay, Y.W.D.; Tan, M.J. Additive manufacturing of geopolymer for sustainable built environment. *J. Clean. Prod.* **2017**, *167*, 281–288.
51. Cao, M.; Xu, L.; Zhang, C. Review on micromechanical design, performance and development tendency of engineered cementitious composite. *J. Chin. Ceram. Soc.* **2015**, *43*, 632–642.
52. Shafei, B.; Kazemian, M.; Dopko, M.; Najimi, M. State-of-the-art review of capabilities and limitations of polymer and glass fibers used for fiber-reinforced concrete. *Materials* **2021**, *14*, 409. [CrossRef]
53. Arisoy, B.; Wu, H.-C. Material characteristics of high performance lightweight concrete reinforced with PVA. *Constr. Build. Mater.* **2008**, *22*, 635–645. [CrossRef]
54. Kizilkanat, A.B.; Kabay, N.; Akyüncü, V.; Chowdhury, S.; Akça, A.H. Mechanical properties and fracture behavior of basalt and glass fiber reinforced concrete: An experimental study. *Constr. Build. Mater.* **2015**, *100*, 218–224. [CrossRef]
55. Zhang, Z.; Zhang, Q. Matrix tailoring of Engineered Cementitious Composites (ECC) with non-oil-coated, low tensile strength PVA fiber. *Constr. Build. Mater.* **2018**, *161*, 420–431. [CrossRef]
56. Singh, A.; Liu, Q.; Xiao, J.; Lyu, Q. Mechanical and macrostructural properties of 3D printed concrete dosed with steel fibers under different loading direction. *Constr. Build. Mater.* **2022**, *323*, 126616.
57. Yang, Y.; Wu, C.; Liu, Z.; Wang, H.; Ren, Q. Mechanical anisotropy of ultra-high performance fibre-reinforced concrete for 3D printing. *Cem. Concr. Compos.* **2022**, *125*, 104310. [CrossRef]
58. Ye, J.; Cui, C.; Yu, J.; Yu, K.; Dong, F. Effect of polyethylene fiber content on workability and mechanical-anisotropic properties of 3D printed ultra-high ductile concrete. *Constr. Build. Mater.* **2021**, *281*, 122586.
59. Ma, H.; Zhang, Z. Paving an engineered cementitious composite (ECC) overlay on concrete airfield pavement for reflective cracking resistance. *Constr. Build. Mater.* **2020**, *252*, 119048. [CrossRef]
60. Zhang, Z.; Yuvaraj, A.; Di, J.; Qian, S. Matrix design of light weight, high strength, high ductility ECC. *Constr. Build. Mater.* **2019**, *210*, 188–197. [CrossRef]
61. Wang, Y.; Liu, F.; Yu, J.; Dong, F.; Ye, J. Effect of polyethylene fiber content on physical and mechanical properties of engineered cementitious composites. *Constr. Build. Mater.* **2020**, *251*, 118917. [CrossRef]

62. Wang, Y.; Zhang, Z.; Yu, J.; Xiao, J.; Xu, Q. Using green supplementary materials to achieve more ductile ECC. *Materials* **2019**, *12*, 858. [CrossRef] [PubMed]
63. Zhang, Z.; Hu, J.; Ma, H. Feasibility study of ECC with self-healing capacity applied on the long-span steel bridge deck overlay. *Int. J. Pavement Eng.* **2019**, *20*, 884–893. [CrossRef]
64. Li, L.; Xiao, B.; Fang, Z.; Xiong, Z.; Chu, S.; Kwan, A. Feasibility of glass/basalt fiber reinforced seawater coral sand mortar for 3D printing. *Addit. Manuf.* **2021**, *37*, 101684.
65. Younis, A.; Ebead, U.; Suraneni, P.; Nanni, A. Fresh and hardened properties of seawater-mixed concrete. *Constr. Build. Mater.* **2018**, *190*, 276–286.
66. Wang, Z.; Zhao, X.-L.; Xian, G.; Wu, G.; Raman, R.S.; Al-Saadi, S. Effect of sustained load and seawater and sea sand concrete environment on durability of basalt-and glass-fibre reinforced polymer (B/GFRP) bars. *Corros. Sci.* **2018**, *138*, 200–218.
67. Yang, S.; Xu, J.; Zang, C.; Li, R.; Yang, Q.; Sun, S. Mechanical properties of alkali-activated slag concrete mixed by seawater and sea sand. *Constr. Build. Mater.* **2019**, *196*, 395–410. [CrossRef]
68. Zhou, A.; Qin, R.; Chow, C.L.; Lau, D. Structural performance of FRP confined seawater concrete columns under chloride environment. *Compos. Struct.* **2019**, *216*, 12–19. [CrossRef]
69. Chu, S.; Li, L.; Kwan, A. Development of extrudable high strength fiber reinforced concrete incorporating nano calcium carbonate. *Addit. Manuf.* **2021**, *37*, 101617. [CrossRef]
70. Lampropoulos, A.; Paschalis, S.A.; Tsioulou, O.; Dritsos, S.E. Strengthening of reinforced concrete beams using ultra high performance fibre reinforced concrete (UHPFRC). *Eng. Struct.* **2016**, *106*, 370–384.
71. Yu, K.; Li, L.; Yu, J.; Xiao, J.; Ye, J.; Wang, Y. Feasibility of using ultra-high ductility cementitious composites for concrete structures without steel rebar. *Eng. Struct.* **2018**, *170*, 11–20. [CrossRef]
72. Kwan, A.; Chu, S. Direct tension behaviour of steel fibre reinforced concrete measured by a new test method. *Eng. Struct.* **2018**, *176*, 324–336.
73. Chu, S.; Kwan, A. Mixture design of self-levelling ultra-high performance FRC. *Constr. Build. Mater.* **2019**, *228*, 116761.
74. Sun, X.; Zhou, J.; Wang, Q.; Shi, J.; Wang, H. PVA fibre reinforced high-strength cementitious composite for 3D printing: Mechanical properties and durability. *Addit. Manuf.* **2022**, *49*, 102500. [CrossRef]
75. Chen, M.; Yang, L.; Zheng, Y.; Li, L.; Wang, S.; Huang, Y.; Zhao, P.; Lu, L.; Cheng, X. Rheological behaviors and structure build-up of 3D printed polypropylene and polyvinyl alcohol fiber-reinforced calcium sulphoaluminate cement composites. *J. Mater. Res. Technol.* **2021**, *10*, 1402–1414. [CrossRef]
76. Teixeira, R.S.; Santos, S.F.d.; Christoforo, A.L.; Savastano Jr, H.; Lahr, F.A.R. Extrudability of cement-based composites reinforced with curauá (Ananas erectifolius) or polypropylene fibers. *Constr. Build. Mater.* **2019**, *205*, 97–110. [CrossRef]
77. Zhang, Y.; Aslani, F. Development of fibre reinforced engineered cementitious composite using polyvinyl alcohol fibre and activated carbon powder for 3D concrete printing. *Constr. Build. Mater.* **2021**, *303*, 124453. [CrossRef]
78. Sun, J.; Aslani, F.; Lu, J.; Wang, L.; Huang, Y.; Ma, G. Fibre-reinforced lightweight engineered cementitious composites for 3D concrete printing. *Ceram. Int.* **2021**, *47*, 27107–27121. [CrossRef]
79. Wang, D.; Ju, Y.; Shen, H.; Xu, L. Mechanical properties of high performance concrete reinforced with basalt fiber and polypropylene fiber. *Constr. Build. Mater.* **2019**, *197*, 464–473. [CrossRef]
80. Kazemian, A.; Yuan, X.; Cochran, E.; Khoshnevis, B. Cementitious materials for construction-scale 3D printing: Laboratory testing of fresh printing mixture. *Constr. Build. Mater.* **2017**, *145*, 639–647. [CrossRef]
81. Mechtcherine, V.; Nerella, V.N.; Kasten, K. Testing pumpability of concrete using Sliding Pipe Rheometer. *Constr. Build. Mater.* **2014**, *53*, 312–323. [CrossRef]
82. Yu, K.; McGee, W.; Ng, T.Y.; Zhu, H.; Li, V.C. 3D-printable engineered cementitious composites (3DP-ECC): Fresh and hardened properties. *Cem. Concr. Res.* **2021**, *143*, 106388. [CrossRef]
83. Tran, M.V.; Cu, Y.T.; Le, C.V. Rheology and shrinkage of concrete using polypropylene fiber for 3D concrete printing. *J. Build. Eng.* **2021**, *44*, 103400. [CrossRef]
84. Koehler, E.P.; Fowler, D.W.; Ferraris, C.F.; Amziane, S. A new, portable rheometer for fresh self-consolidating concrete. *Aci Spec. Publ.* **2005**, *233*, 97.
85. Pham, L.; Tran, P.; Sanjayan, J. Steel fibres reinforced 3D printed concrete: Influence of fibre sizes on mechanical performance. *Constr. Build. Mater.* **2020**, *250*, 118785. [CrossRef]
86. Le Hoang, A.; Fehling, E. Influence of steel fiber content and aspect ratio on the uniaxial tensile and compressive behavior of ultra high performance concrete. *Constr. Build. Mater.* **2017**, *153*, 790–806. [CrossRef]
87. Meng, W.; Khayat, K.H. Effect of hybrid fibers on fresh properties, mechanical properties, and autogenous shrinkage of cost-effective UHPC. *J. Mater. Civ. Eng.* **2018**, *30*, 04018030. [CrossRef]
88. Ma, G.; Li, Z.; Wang, L.; Wang, F.; Sanjayan, J. Mechanical anisotropy of aligned fiber reinforced composite for extrusion-based 3D printing. *Constr. Build. Mater.* **2019**, *202*, 770–783. [CrossRef]
89. Le, T.T.; Austin, S.A.; Lim, S.; Buswell, R.A.; Law, R.; Gibb, A.G.; Thorpe, T. Hardened properties of high-performance printing concrete. *Cem. Concr. Res.* **2012**, *42*, 558–566. [CrossRef]
90. Arunothayan, A.R.; Nematollahi, B.; Ranade, R.; Bong, S.H.; Sanjayan, J. Development of 3D-printable ultra-high performance fiber-reinforced concrete for digital construction. *Constr. Build. Mater.* **2020**, *257*, 119546. [CrossRef]

91. Arunothayan, A.R.; Nematollahi, B.; Ranade, R.; Khayat, K.H.; Sanjayan, J.G. Digital fabrication of eco-friendly ultra-high performance fiber-reinforced concrete. *Cem. Concr. Compos.* **2022**, *125*, 104281. [CrossRef]
92. Ma, G.; Li, Z.; Wang, L.; Bai, G. Micro-cable reinforced geopolymer composite for extrusion-based 3D printing. *Mater. Lett.* **2019**, *235*, 144–147. [CrossRef]
93. Bos, F.; Bosco, E.; Salet, T. Ductility of 3D printed concrete reinforced with short straight steel fibers. *Virtual Phys. Prototyp.* **2019**, *14*, 160–174. [CrossRef]
94. Liu, Y.; Shi, C.; Zhang, Z.; Li, N.; Shi, D. Mechanical and fracture properties of ultra-high performance geopolymer concrete: Effects of steel fiber and silica fume. *Cem. Concr. Compos.* **2020**, *112*, 103665. [CrossRef]
95. Yang, Y.; Wu, C.; Liu, Z.; Li, J.; Yang, T.; Jiang, X. Characteristics of 3D-printing ultra-high performance fibre-reinforced concrete under impact loading. *Int. J. Impact Eng.* **2022**, *164*, 104205. [CrossRef]
96. Zhou, J.; Lai, J.; Du, L.; Wu, K.; Dong, S. Effect of directionally distributed steel fiber on static and dynamic properties of 3D printed cementitious composite. *Constr. Build. Mater.* **2022**, *318*, 125948. [CrossRef]
97. Lim, J.H.; Panda, B.; Pham, Q.-C. Improving flexural characteristics of 3D printed geopolymer composites with in-process steel cable reinforcement. *Constr. Build. Mater.* **2018**, *178*, 32–41. [CrossRef]
98. Ding, T.; Xiao, J.; Zou, S.; Yu, J. Flexural properties of 3D printed fibre-reinforced concrete with recycled sand. *Constr. Build. Mater.* **2021**, *288*, 123077. [CrossRef]
99. Koenders, E.A.; Pepe, M.; Martinelli, E. Compressive strength and hydration processes of concrete with recycled aggregates. *Cem. Concr. Res.* **2014**, *56*, 203–212. [CrossRef]
100. Xiao, J.; Zou, S.; Ding, T.; Duan, Z.; Liu, Q. Fiber-reinforced mortar with 100% recycled fine aggregates: A cleaner perspective on 3D printing. *J. Clean. Prod.* **2021**, *319*, 128720. [CrossRef]
101. Xiao, J.; Li, W.; Fan, Y.; Huang, X. An overview of study on recycled aggregate concrete in China (1996–2011). *Constr. Build. Mater.* **2012**, *31*, 364–383. [CrossRef]
102. Ding, T.; Xiao, J.; Zou, S.; Zhou, X. Anisotropic behavior in bending of 3D printed concrete reinforced with fibers. *Compos. Struct.* **2020**, *254*, 112808. [CrossRef]
103. Cai, J.; Sheng, Z.; Wang, X.; Fang, Y.; Pan, J. Effect of reinforcement configurations on the flexural behaviors of 3D printed fiber reinforced cementitious composite (FRCC) beams. *J. Build. Eng.* **2022**, *46*, 103773. [CrossRef]
104. Bos, F.P.; Ahmed, Z.Y.; Jutinov, E.R.; Salet, T.A. Experimental exploration of metal cable as reinforcement in 3D printed concrete. *Mater. Lett.* **2017**, *10*, 1314. [CrossRef]
105. Marchment, T.; Sanjayan, J. Mesh reinforcing method for 3D Concrete Printing. *Autom. Constr.* **2020**, *109*, 102992. [CrossRef]
106. Gebhard, L.; Mata-Falcón, J.; Anton, A.; Burger, J.; Lloret-Fritschi, E.; Reiter, L.; Dillenburger, B.; Gramazio, F.; Kohler, M.; Flatt, R. Aligned interlayer fibre reinforcement and post-tensioning as a reinforcement strategy for digital fabrication. In Proceedings of the RILEM International Conference on Concrete and Digital Fabrication, Eindhoven, The Netherlands, 6–8 July 2020; pp. 622–631.
107. Xiao, J.; Han, N.; Zhang, L.; Zou, S.J.C.; Materials, B. Mechanical and microstructural evolution of 3D printed concrete with polyethylene fiber and recycled sand at elevated temperatures. *Constr. Build. Mater.* **2021**, *293*, 123524. [CrossRef]
108. Shakor, P.; Nejadi, S.; Paul, G. An investigation into the behaviour of cementitious mortar in the construction of 3D printed members by the means of extrusion printing. In Proceedings of the 1st International Conference on 3D Construction Printing, Melbourne, Australia, 26–28 November 2018.
109. Lim, J.H.; Li, M.; Weng, Y. Effect of fiber reinforced polymer on mechanical performance of 3D printed cementitious material. In Proceedings of the Proceedings of the International Conference on Progress in Additive Manufacturing, Singapore, 14–17 May 2018; pp. 44–49.
110. Jin, Y.; Zhou, X.; Chen, M.; Zhao, Z.; Huang, Y.; Zhao, P.; Lu, L. High toughness 3D printed white Portland cement-based materials with glass fiber textile. *Mater. Lett.* **2022**, *309*, 131381. [CrossRef]
111. Wang, L.; Zeng, X.; Li, Y.; Yang, H.; Tang, S. Influences of MgO and PVA fiber on the abrasion and cracking resistance, pore structure and fractal features of hydraulic concrete. *Fractal Fract.* **2022**, *6*, 674. [CrossRef]
112. Wang, L.; Guo, F.; Yang, H.; Wang, Y.; Tang, S. Comparison of fly ash, PVA fiber, MgO and shrinkage-reducing admixture on the frost resistance of face slab concrete via pore structural and fractal analysis. *Fractals* **2021**, *29*, 2140002. [CrossRef]
113. Sun, X.; Gao, C.; Wang, H. Bond performance between BFRP bars and 3D printed concrete. *Constr. Build. Mater.* **2021**, *269*, 121325. [CrossRef]
114. van den Heever, M.; du Plessis, A.; Kruger, J.; van Zijl, G. Evaluating the effects of porosity on the mechanical properties of extrusion-based 3D printed concrete. *Cem. Concr. Res.* **2022**, *153*, 106695. [CrossRef]
115. Nematollahi, B.; Vijay, P.; Sanjayan, J.; Nazari, A.; Xia, M.; Naidu Nerella, V.; Mechtcherine, V. Effect of polypropylene fibre addition on properties of geopolymers made by 3D printing for digital construction. *Mater. Lett.* **2018**, *11*, 2352. [CrossRef] [PubMed]
116. Nematollahi, B.; Sanjayan, J.; Qiu, J.; Yang, E.-H. High ductile behavior of a polyethylene fiber-reinforced one-part geopolymer composite: A micromechanics-based investigation. *Arch. Civ. Mech. Eng.* **2017**, *17*, 555–563. [CrossRef]
117. Nematollahi, B.; Sanjayan, J.; Qiu, J.; Yang, E.-H. Micromechanics-based investigation of a sustainable ambient temperature cured one-part strain hardening geopolymer composite. *Constr. Build. Mater.* **2017**, *131*, 552–563. [CrossRef]
118. Nematollahi, B.; Xia, M.; Sanjayan, J.; Vijay, P. Effect of type of fiber on inter-layer bond and flexural strengths of extrusion-based 3D printed geopolymer. *Mater. Sci. Forum.* **2018**, *939*, 155–162. [CrossRef]

119. Lesovik, V.; Fediuk, R.; Amran, M.; Alaskhanov, A.; Volodchenko, A.; Murali, G.; Uvarov, V.; Elistratkin, M. 3D-Printed Mortars with Combined Steel and Polypropylene Fibers. *Fibers* **2021**, *9*, 79. [CrossRef]
120. Nematollahi, B.; Ranade, R.; Sanjayan, J.; Ramakrishnan, S. Thermal and mechanical properties of sustainable lightweight strain hardening geopolymer composites. *Arch. Civ. Mech. Eng.* **2017**, *17*, 55–64. [CrossRef]
121. Akhlaghi, M.A.; Bagherpour, R.; Kalhori, H. Application of bacterial nanocellulose fibers as reinforcement in cement composites. *Constr. Build. Mater.* **2020**, *241*, 118061. [CrossRef]
122. Alamshahi, V.; Taeb, A.; Ghaffarzadeh, R.; Rezaee, M.A. Effect of composition and length of PP and polyester fibres on mechanical properties of cement based composites. *Constr. Build. Mater.* **2012**, *36*, 534–537. [CrossRef]
123. Scheurer, M.; Quenzel, P.; Nölke, P.; Reuter-Schniete, J.; Gries, T. Investigating the feasibility of using carbon fiber tapes as reinforcement for 3D concrete printing. *Civ. Eng. Des.* **2021**, *3*, 136–142. [CrossRef]
124. Kühn, F.; Rehra, J.; May, D.; Schmeer, S.; Mitschang, P. Dry fiber placement of carbon/steel fiber hybrid preforms for multifunctional composites. *Adv. Manuf. Polym. Compos. Sci.* **2019**, *5*, 37–49. [CrossRef]
125. Rutzen, M.; Schulz, M.; Moosburger-Will, J.; Lauff, P.; Fischer, O.; Volkmer, D. 3D printing as an automated manufacturing method for a carbon fiber-reinforced cementitious composite with outstanding flexural strength (105 N/mm^2). *Mater. Struct.* **2021**, *54*, 1–20. [CrossRef]
126. Sumesh, M.; Alengaram, U.J.; Jumaat, M.Z.; Mo, K.H.; Alnahhal, M.F. Incorporation of nano-materials in cement composite and geopolymer based paste and mortar–A review. *Constr. Build. Mater.* **2017**, *148*, 62–84. [CrossRef]
127. Emdadi, Z.; Asim, N.; Amin, M.H.; Ambar Yarmo, M.; Maleki, A.; Azizi, M.; Sopian, K. Development of green geopolymer using agricultural and industrial waste materials with high water absorbency. *Appl. Sci.* **2017**, *7*, 514. [CrossRef]
128. Lee, N.; Kim, E.; Lee, H.-K. Mechanical properties and setting characteristics of geopolymer mortar using styrene-butadiene (SB) latex. *Constr. Build. Mater.* **2016**, *113*, 264–272. [CrossRef]
129. Zhang, Z.-H.; Yao, X.; Zhu, H.-J.; Hua, S.-D.; Chen, Y. Preparation and mechanical properties of polypropylene fiber reinforced calcined kaolin-fly ash based geopolymer. *J. Cent. South Univ. Technol.* **2009**, *16*, 49–52. [CrossRef]

Disclaimer/Publisher's Note: The statements, opinions and data contained in all publications are solely those of the individual author(s) and contributor(s) and not of MDPI and/or the editor(s). MDPI and/or the editor(s) disclaim responsibility for any injury to people or property resulting from any ideas, methods, instructions or products referred to in the content.